Early Cardiac Mitochondrial Dysfunction in the Nile Rat model of Type 2 Diabetes

by:

Jillian Frances Schneider

A thesis submitted in partial fulfillment of the requirements for the degree of:

Master of Science

Department of Physiology
University of Alberta

Abstract

The pathological events initiating diabetic cardiac changes in response to chronic hyperglycemia and hyperinsulinemia remain unclear. Due to the high metabolic activity of the heart, and its sensitivity to acute changes in oxygen and substrate flux, mitochondrial dysfunction has been proposed as a potential early indicator of diabetic cardiac disease. We hypothesize that mitochondrial changes in cardiac tissue will precede the onset of hyperglycemia in the Nile grass rat (NR), a model of spontaneous Type 2 diabetes. Male NRs were fed standard rodent chow (Prolab 2000) or a high fibre low fat diet (Mazuri Chinchilla). Hearts were studied at 2, 6, 12 (echo only) and 18 months. Mitochondrial dysfunction was assessed in permeabilized cardiac fibres utilizing the OROBOROS Oxygraph-2k high-resolution respirometry system. Four protocols were applied, including two states: LEAK state (non-phosphorylating, ADP-free) and the oxidative phosphorylation state, measuring oxygen consumption coupled to the phosphorylation of ADP to ATP. We used substrates feeding electrons into Complexes I (NADH-pathway), II (Succinate pathway) or IV of the electron transport system. Mitochondrial metabolism for fatty acids octanoylcarnitine, palmitoylcarnitine, and acetylcarnitine was similarly assessed. Additional testing included citrate synthase activity, glycated hemoglobin A1c, plasma insulin levels, and transthoracic echocardiography. Echocardiography results were suggestive of mild diastolic dysfunction at 12 months of age. Hyperglycemia and elevated %HbA1c were noted in Prolab-fed animals after 6 months, preceded by hyperinsulinemia detectable at 2 months. High resolution respirometry results showed an increase in the flux control ratio of Complex IV and citrate enzymatic assay results suggest an increase in mitochondrial content in Prolab-fed animals at 2 months. This preceded the onset of hyperglycemia, but not hyperinsulinemia. Other dietary and aging-related changes were noted in mitochondrial LEAK and OXPHOS

capacities per mg permeabilized fibres at 6 and 18 months, and an increase in fatty acid β-oxidation (FAO) for medium-chain fatty acids was observed at 6 months. These results suggest that mitochondrial functional changes are detectable prior to the onset of hyperglycemia in the NR, and these dysfunctions coincide with the onset of hyperinsulinemia.

Preface

This thesis is an original work by Jillian Frances Schneider. The research project on which this thesis is based received ethics approval from the University of Alberta Research Ethics Board, Project name "Early Cardiac Mitochondrial Dysfunction in the Nile Rat model of Type 2 Diabetes", AUP#00000328, January 2016.

Acknowledgments

I would like to extend my deepest thanks to my supervisor Dr. Yves Sauvé, for his patience, expert guidance, and willingness to take on this ambitious project. Without his constant support, advice, and special dash of humour, this project would never have been possible. I have grown as a researcher thanks to his passion for research, and I am grateful to have had the opportunity to study under him. I would also like to thank my supervisor, Dr. Hélène Lemieux, for her kindness, patience, and never-ending knowledge in all things mitochondria. Her attention to detail and passion for her field inspired me to learn as much as I could, which has only made me a stronger researcher.

I am grateful for the inputs of my committee members, Dr. Cathy Chan and Dr. Rick Shultz, and my external examiner, Dr. Gabor Gyenes. Their insights and feedback during meetings was greatly appreciated, and their knowledge of their respective fields was invaluable.

I would like to thank all members of the Sauvé lab – Sharee Kuny, Dr. Camille Dejos, and Ted Han, for their respective contributions to this project. I would also like to thank Donna Beker for her contributions to the echocardiography studies on the Nile Rats.

All work reported was supported by the Canadian Institutes of Health Research (CIHR), the Frederick Banting and Charles Best Canada Graduate Scholarship, and the Queen Elizabeth II Graduate Scholarship.

Table of Contents

List of Figures

List of Tables

A.1 Chapter 1- INTRODUCTION

A.1.1 Diabetes Mellitus

The global health burden of diabetes mellitus (DM) has increased significantly over the last 50 years and is anticipated to continue rising[1]. The International Diabetes Federation (IDF) has classified the DM epidemic as a global emergency, estimating that approximately 415 million people worldwide live with DM[1]. This figure is anticipated to rise to 642 million by the year 2040. Affecting one in every 11 adults worldwide in 2015, estimates indicate that one person dies every six seconds from complications relating to DM. Furthermore, approximately 318 million adults display aggravated glucose intolerance, which puts them at risk for developing DM in the future[1]. Although Canada does not rank in the top ten countries for adults with DM, prevalence is increasing; approximately 3.4 million Canadians live with DM, and Canadian statistics predict a 44% increase in DM cases between 2015 and 2035. Despite treatment developments and global awareness initiatives, the number of individuals afflicted with DM continues to grow, posing a serious risk to the stability of the Canadian and global health care systems[2].

DM is a metabolic disorder characterized by chronic hyperglycemia with disturbances in carbohydrate, protein, and fat metabolism, secondary to disrupted insulin secretion or action[3]. DM is divided into two subtypes. Type 1 diabetes mellitus (T1DM) describes diabetic hyperglycemia secondary to autoimmune beta cell destruction, whereby patients are largely aninsulinemic (lacking endogenous insulin production) and thus become insulin dependent. Type 2 diabetes mellitus (T2DM) describes an "insulin-independent" phenotype. Patients may present with insulin resistance combined with normal insulin levels or relative hyperinsulinemia; alternatively, patients may develop insulin secretory deficits,

leading to hypoinsulinemia[4]. The prevalence of T2DM significantly exceeds that of T1DM, accounting for up to 85 – 90% of diagnosed cases[3]. This is likely exacerbated by poor dietary habits, and the sedentary lifestyles more characteristic of modern nations, although family history of T2DM, hypertension, and dyslipidemia are also significant risk factors for disease onset[5].

Clinically, diabetic patients may present with chronic thirst, polyuria, blurred vision, and weight loss; in severe cases, patients may show signs of ketoacidosis, and require emergency treatment[3]. A clinical diagnosis of diabetes is confirmed with a combination of fasting plasma glucose (FBG) ≥7.0 mmol/L, two hour plasma glucose (2hPG) post 75 g oral glucose tolerance test (OGTT) ≥11.1 mmol/L, or hemoglobin A1c (HbA1c) ≥6.5% (48 mmol/mol) in adults[6]. Patients at risk of developing diabetes are classified as "pre-diabetic", and present with a FBG of 6.1 – 6.9 mmol/L, 2hPG post OGTT of 7.8 – 11.0 mmol/L, or HbA1c of 6.0 - 6.4%. In addition, these individuals may present with other clinical indicators of T2DM, such as obesity, glucosuria, hypertension, or polydipsia. Therefore, annual screening for T2DM in individuals with pertinent family history, and/or clinical risk factors may improve detection[4]. In practice, a diagnosis of diabetes is based on the threshold HbA1c value for developing microvascular disease[4]. Although commonly utilized as a longitudinal marker of glycemic status, HbA1c is a useful diagnostic tool in diabetes management[7]. HbA1c readings represent an average plasma glucose value over a 2-3 month period, and therefore lack the variability occurring in FBG readings over the course of a day[4]. Timely initiation of treatment for T2DM is critical to improve glycemic status, and to reduce the risk of complications. Dietary and lifestyle changes, self-management care, and manual blood glucose testing are frequently recommended as first-line treatments to achieve a target HbA1c of 6-7%, in most patients. If glycemic targets are not met, Canadian Diabetes Clinical

Practice Guidelines recommend adding pharmacological agents best suited to the individual's clinical profile[4]. Metformin is frequently selected as the agent of choice, due to its effectiveness at reducing blood glucose, low incidence of mild side effects, proven cardiovascular benefit, and lack of causing weight gain, not to mention low cost[8]. However, Metformin is not effective in all cases, and is contraindicated in patients with chronic kidney disease, due to a perceived risk of lactic acidosis[9].

A.1.2 Complications of Diabetes

Sustained hyperglycemia in T2DM is associated with the development of severe complications, affecting the heart, eyes, kidneys, peripheral nerves, and liver. According to the IDF, the most prevalent complications include diabetic retinopathy, cardiovascular disease, pregnancy complications (in gestational diabetes, or diabetic women who become pregnant) and diabetic foot disease, with resultant amputations[1]. In the literature, complications are classified as microvascular (retinopathy, neuropathy, or nephropathy), or macrovascular (coronary, cerebrovascular, peripheral) in nature[10]. These complications are commonly associated with patient morbidity and mortality, respectively. Furthermore, complications increase physical and psychological burdens on patients, who must adapt their lifestyle to accommodate dietary restrictions, frequent visits to a primary care provider and the additional stress associated with managing a chronic disease. Other bodily systems affected by T2DM (digestive, hepatic, and musculo-skeletal) may lead to complications including gastroparesis (secondary to vagal nerve damage), liver cirrhosis (secondary to non-alcoholic fatty liver disease) and cheiroarthropathy (limited joint mobility of the hands)[11], respectively. Further studies also indicate that T2DM is associated with changes in cognitive functioning and increased susceptibility to pancreatic and colorectal cancers[12,13]. Primary management of these patients involves promptly reducing their glucose level(targets

determined by age and risk status), cardiovascular risk factors, and HbA1c percentage[4]. There is consensus that aggressive glycemic control and reduction of HbA1c provides a relative risk-reduction of diabetes-related death, and reduced incidence of major microvascular complications[14,15]. The effect of aggressive glycemic control on macrovascular complications is still in question. While some studies have shown benefits, others have reported significant harm, leading to discontinuation of treatment[16]. Multi-drug regimens may be beneficial in older patients, or in those with significant co-morbidities, as they facilitate management of multiple complications; however, these regimens may reduce patient compliance and drug adherence[17]. Contributors to poor compliance include, lack of confidence in future drug benefits, poor understanding of the purpose for treatment and prolonged course of treatment, which must be managed by the prescriber[18]. Therefore, finding a balance of appropriate management with thorough patient education and compliance is key to preventing the onset of further complications.

A.1.3 Cardiovascular Complications of Diabetes

T2DM is a major risk factor for cardiovascular disease, such that cardiovascular complications are the leading cause of morbidity and mortality in DM patients. People afflicted with DM are 2-4 times more likely to develop cardiovascular disease, and over three times more likely to be hospitalized secondary to cardiac problems[19]. DM also increases heart failure risk 4-fold, even after adjustment for standard risk factors[20]. Cardiac complications include may include systolic and diastolic dysfunctions[21,22], left ventricular hypertrophy[23], atherosclerosis[24], atrial fibrosis and fibrillation[25], and myocardial infarction[26]. Increasing T2DM awareness and prophylactic treatment approaches have significantly improved patient outcomes; recent data suggests that the rate of myocardial infarction in DM patients in the US has decreased by 68% from 1990 to 2010[27]. Diabetes-induced cardiovascular disease may

stem from different causes, such as: 1) coronary atherosclerosis associated with risk factors (obesity, hyperlipidemia, and hypertension); 2) microangiopathy of cardiac microvasculature; 3) cardiac dysfunction in the absence of coronary artery disease and hypertension, termed "diabetic cardiomyopathy". Although ischemic heart disease is acknowledged as the most common cause of death in persons with diabetes, diabetic cardiomyopathy is becoming increasingly recognized as a clinically significant entity[28].

A.1.4 Diabetic Cardiomyopathy

Diabetic cardiomyopathy (DCM) is clinically defined as biochemical, morphological, and functional myocardial changes in the absence of coronary artery disease (CAD), hypertension, and significant valvular disease[9, 25,29,30,]. DCM was first described by Rubler *et al.* in 1972*,* who reported four diabetic patients who died of heart failure, without displaying signs of CAD[31]. A widely accepted clinical definition of DCM remains undefined, and clinicians may rely on disparate criteria when making a diagnosis. DCM patients may present asymptomatically, or may be short of breath with a combination of non-specific symptoms, including weakness, fatigue, and ankle edema. However, this presentation is highly variable and remains a puzzle for clinicians[32]. The most common cardiac clinical features of DCM are diastolic dysfunction and left ventricular hypertrophy. However, cardiac studies of DCM patients also report subclinical systolic dysfunction, and coronary microvascular dysfunction[30]. Estimates of DCM prevalence vary among the diabetic population, with reports ranging from 30 up to 75%[33]. Patients with DCM are at risk of adverse outcomes, such as late-stage systolic dysfunction, progressive cardiac failure, and death[33].

The molecular basis for the onset of diabetic cardiomyopathy remains uncertain. Various contributing pathways have been studied in isolation, and their combined effects on cardiac muscle likely contribute to the development of DCM. Advanced glycation end

products (AGEs) have been implicated in the development of ventricular dysfunction in T2DM. AGEs are formed by glycation, where a protein or lipid molecule becomes covalently bonded to a carbohydrate molecule, such as glucose. Chronic hyperglycemia accelerates AGE formation, which leads to their increased deposition in various organs, including the heart[34]. AGEs may increase left ventricular (LV) stiffness directly by cross-linking myocardial collagen or other extracellular matrix proteins, directly affecting diastolic and/or systolic function[34]. A sustained increase in mitochondrial fatty acid oxidation (FAO) has also been discussed as a significant contributor to cardiac metabolic remodelling in T2DM. High dietary fat contributes to increasing plasma fatty acids (FAs), leading to increased cellular and mitochondrial uptake of FAs. Loss of malonyl-CoA-mediated inhibition of carnitine palmitoyl transferase (CPT1) may contribute to increased mitochondrial uptake of FAs, due to an increase in malonyl-CoA decarboxylase (MCD) in DM. MCD is the enzyme responsible for the degradation of malonyl-CoA in the heart[35,36]. Chronic influx of FAs shifts substrate utilization towards increased oxidation of FAs, and decreased glucose oxidation in the heart. This shift is perpetuated by intercellular hyperglycemia, and insulin resistance[20]. Enhanced myocardial FAO occurs with the activation of peroxisome-proliferator activated receptor α (PPARα). PPARα is a transcription factor involved in myocardial regulation of FA oxidation rates[37]. Cardiac overexpression of PPARα induces a diabetes-like state, with combined increase in FAO and decline in both glucose uptake and oxidation[37]. Activation of PPARα indirectly promotes the accumulation of toxic ceramides and diacylglycerol through activation of protein kinase c (PKC), which compromises the viability of cardiac cells, and may contribute to cardiac dysfunction[38]. PKC activation has also been shown to perpetuate insulin resistance by

reducing insulin signalling through phosphorylation at the insulin receptor, and reducing the translocation of glucose transporter 4 (GLUT4)[39].

Schilling *et al.* have presented a hypothesis implicating mitochondrial dysfunction directly at the center of the pathogenesis of DCM[40]. They discuss three discrete phases – a compensated phase, transition phase, and decompensated phase – whereby mitochondrial management of FAO within the cardiomyocyte is progressively dysregulated in DM, leading to reactive oxygen species (ROS) accumulation, disruption of triacylglycerol (TAG) synthesis, and eventual myocardial contractile dysfunction and fibrosis[40]. Additional studies also discuss the role of mitochondrial changes in the pathogenesis of diabetic cardiac disease[41–43]. Although promising, further studies investigating prodromal stages of diabetic heart disease, and measuring several markers of mitochondrial function/oxidative stress are required to clarify the mechanistic progression of DCM.

A.1.5 Echocardiographic Assessment of the Diabetic Heart

Echocardiography is a standard imaging modality utilized clinically to directly visualize cardiac function. It is safe, non-invasive, and relatively inexpensive, making it a useful imaging technique among clinicians and researchers. Routine echocardiography involves directing high frequency two-dimensional, three dimensional, or Doppler ultrasound waves at the tissue of interest, using a handheld probe. A transthoracic approach is commonly used to image the heart; alternatively, clinicians may utilize a trans-esophageal approach if transthoracic images are inadequate, or if more precise visualization of aortic and atrial structures is required. The resulting images allow clinicians to visualize the dimensions of the cardiac muscle, quantify internal chamber size, assess mechanical pumping capabilities, and quantify the direction and velocity of blood flow[44]. Echocardiograms are an invaluable diagnostic tool for serial monitoring of cardiac functional changes in DM patients.

At very early stages of diabetic cardiac disease, damage to cardiomyocytes is subcellular, meaning that echocardiographic findings are not apparent; however, this is not sufficient to rule out a diagnosis of DCM, as overt changes often arise later in disease progression[45]. Diastolic dysfunction is frequently the initial abnormality detected on echocardiography in DCM patients. By definition, diastolic dysfunction implies that the cardiac ejection fraction is preserved, while cardiac relaxation is disrupted. Studies have reported a prevalence of diastolic dysfunction in up to 30% of T2DM patients; however, this may be underrepresented, as studies utilizing tissue Doppler imaging (TDI) have reported up to 75% prevalence in T2DM patients[46]. Echocardiographic evaluation of diastolic dysfunction is commonly performed using transmitral inflow Doppler imaging, whereby the velocity of blood flow through the mitral valve is measured. Mitral inflow imaging permits the analysis of functional variables, such as the E-wave, the A-wave, and isovolumic relaxation time (IVRT), among many others[45,47]. The E-wave and A-wave refer to peak early, and late (atrial) diastolic filling (respectively). In a healthy individual, the E-wave is greater than the A-wave. IVRT is a marker of myocardial relaxation, and refers to the interval between the closure of the aortic valve, and the opening of the mitral valve (indicating filling onset)[48]. In the initial stages of diastolic dysfunction, the IVRT will become prolonged (>200 ms), and the E/A ratio will fall below 1, due to a slower E-wave and a faster A-wave. This is suggestive of abnormal relaxation of LV myocardium[47]. Additional outcome variables for diastolic dysfunction may include changes in mitral inflow with the Valsalva maneuver, pulmonary venous flow monitoring, color M-mode flow propagation velocity, or early and late mitral tissue velocities using tissue Doppler imaging (TDI)[47].

An additional useful diagnostic parameter in diabetic patients is the assessment of LV dimensions. Changes in LV size and compliance are acknowledged contributors to the

progression of diastolic dysfunction, as a stiff or oversized ventricle may impair ventricular relaxation. Left ventricular hypertrophy (LVH) and increased LV wall thickness are known to occur in patients with both T1DM and T2DM; in a study of 294 patients with T2DM, 56% were reported to have LVH, although this varied by BMI and hypertensive status[49]. Larger studies have shown that T2DM patients have up to a 1.5-fold increased risk of developing LVH, when compared to non-diabetic controls[50]. Impairment of LV function may arise by various mechanisms, including systemic hypertension, microangiopathy, increased extracellular collagen deposition, or left atrial dysfunction, all of which may occur in diabetic patients[51,52]. LVH can be evaluated using two-dimensional echocardiography (parasternal long axis views) to measure interventricular septal wall thickness, LV internal diameter and LV posterior wall thickness. Approximate LV mass can be calculated formulaically, when indexed by patient height[23]. Additional variables and recommendations for thorough evaluation of left ventricular function are reviewed elsewhere[53].

A.1.6 Mitochondrial Physiology

Given their primordial function in aerobic metabolism, mitochondria are of major interest to the pathogenesis of T2DM and its complications. Considered the energetic powerhouse of eukaryotic cells, mitochondria are double membrane-bound organelles that consume oxygen, electrons, and physiological intermediates to stimulate biosynthetic reactions, ultimately generating adenosine triphosphate (ATP)[30]. They also play host to important biochemical circuits, such as the TCA or Kreb's cycle, the urea cycle, and ketogenesis[54]. Mitochondria are implicated in cell death signalling[55], cellular metabolism[54], calcium homeostasis[56], and regulation of redox processes[57], and have been studied extensively for their role in disease processes, including neurodegenerative disorders[58,59],

cancers and malignant tumor progression[60,61], insulin resistance[62,63], Type 2 diabetes[41,64], and cardiovascular complications associated with diabetes[65,66,67].

Mitochondria generate energy through a process called oxidative phosphorylation (OXPHOS). In this process, the movement of electrons through the electron transport system (ETS) is coupled with the production of energy in the form of ATP by ATP synthase. The ETS is comprised of four multi-protein complexes, each containing several specific electron carriers. Respiratory complexes I (NADH dehydrogenase), II (succinate dehydrogenase), III (Ubiquinol – cytochrome c oxidoreductase), and IV (cytochrome oxidase) are located in the inner mitochondrial membrane. Lipid-soluble mobile electron carrier co-enzyme Q (ubiquinone) receives electrons from complex I and II, and acts as both a double and single electron carrier. Water-soluble cytochrome *c* receives electrons from complex III, and acts as a single electron carrier. Electrons are passed in sequence from carriers with lower reduction potentials to carriers with higher reduction potentials. Different sources of electrons provide the reducing equivalents to the ETS. Depending on the source, electrons enter the ETS at (1) Complex I (CI, electrons from NADH), (2) Complex II (CII, electrons from succinate), (3) electron-transferring flavoprotein (electrons from $FADH_2$ from fatty acid oxidation), and (4) glycerol-phosphate dehydrogenase (electrons from glycerophosphate). All entering electrons then converge at the Q-junction, and follow a common path to Complex III and Complex IV[68]. At the level of CIV, electrons are transferred to the final electron acceptor oxygen, which is converted to water, and allows the measurement of mitochondrial respiration (mitochondrial oxygen consumption). The energy released by electron transport is harnessed to pump protons from the mitochondrial matrix to the intermembrane space, generating an electrochemical gradient. The chemiosmotic force generated across the inner mitochondrial membrane is harnessed by ATP synthase,

effectively coupling electron transport into the ETS with the phosphorylation of ATP from ADP.

Under normal or pathological conditions, there is a dissipative component to mitochondrial respiration called LEAK respiration, which is in compensation for proton leak (not through ATP synthase), proton slip, cation cycling, and electron leak[69]. This process can be used to produce heat instead of ATP, but may also play an important role in the control of ROS production.

Dietary FAs are an abundant mitochondrial energy source for cardiac metabolism. In healthy hearts, approximately 70% of ATP generated by cardiac mitochondria is generated by FAO[70]. Cytosolic FAs are converted to acyl-CoA by acyl-CoA synthetase, producing fatty acyl-CoA molecules of various lengths. Short and medium-chain FAs (4-12 C) are oxidized in the mitochondria, whereas long-chain FAs (12-16 C) are oxidized in both the mitochondria and the peroxisomes[71]. Short and medium-chain fatty acyl-CoA molecules diffuse through the mitochondrial membrane; however, long-chain fatty acyl-CoA molecules enter the mitochondrion via a carnitine shuttle system to proceed with β-oxidation. Distinct enzymatic activities ensure FA degradation into units of acetyl coenzyme A (acetyl CoA), NADH and $FADH_2$[54]. For example, electrons from $FADH_2$ become available to mitochondria as they are shuttled via the electron transfer protein (ETF) to ubiquinone following the reduction of various chain-length specific FAD dehydrogenases[72].

Electrons for mitochondrial respiration are also available from carbohydrate sources. Increasing systemic glucose levels (i.e. postprandial) initiates intracellular glucose oxidation, generating NADH and pyruvate via glycolysis. Pyruvate is imported into the mitochondrial matrix, transformed into acetyl-CoA by the pyruvate dehydrogenase complex (PDC), and integrated into the Kreb's cycle. The PDC is a large mitochondrial matrix protein that is

necessary for the oxidative decarboxylation of pyruvate within the mitochondria. The complex consists of three catalytic enzymes: pyruvate dehydrogenase (E1), dihydrolipoamide acetyltransferase (E2) and dihydrolipoamide dehydrogenase (E3)[73,74]. These components sequentially process the irreversible decarboxylation of pyruvate, generating acetyl-CoA, NADH, and CO_2[74]. PDC regulation occurs by pyruvate dehydrogenase kinase (PDK) and pyruvate dehydrogenase phosphatase (PDP), which inactivate and activate the complex (respectively) based on fed or fasting status[75]. In a fed state, PDC is phosphorylated, and its activity increases to promote glucose oxidation and energy use. Under fasting conditions, the complex is dephosphorylated and PDC activity is reduced to spare pyruvate for gluconeogenesis[75]. PDC activity is an important upstream contributor to the NADH pathway and CI activity, as it contributes to the reduction of NAD+ to NADH.

A.1.7 Mitochondria and Cardiac Function

Cardiac and mitochondrial metabolism are highly interdependent[76]. In order to beat approximately 100,000 times daily, the human heart consumes up to 6 kg of ATP, the bulk of which is sourced from mitochondria[77]. Mitochondria occupy approximately 30-35% of cardiomyocyte cellular volume, reflecting the high metabolic demands of cardiac cells[78]. Two subpopulations of mitochondria have been identified within cardiac cells: subsarcolemmal mitochondria (SSM) located directly beneath the plasma membrane, and intrafibrillar mitochondria (IFM) located between the myofibrils[79]. SSM mitochondria are more susceptible to the effects of T2DM than IFM mitochondria[80]. The spatial localization of these two subtypes may be indicative of a need to tailor responses to specific physiological stimuli. The effects of changes in glycaemia on cardiac mitochondrial function have been studied in models of both T1DM[81,82] and T2DM[65,83], as well as in humans[80,41,84]. A pervading theory addresses the effects of T2DM on metabolic flexibility in cardiomyocytes, since the

heart is capable of utilizing multiple energy sources, such as FAs, glucose, ketones, lactate, and free amino acids. As mentioned previously, FAO is arguably a predominant contributor to cardiac oxidative energy metabolism, providing up to 70% of cardiac ATP[85]. The usage of energy substrates will vary based on their relative abundance, as well as on metabolic status[85]. Cardiac metabolism is tightly regulated, and responds to multiple factors, such as oxygen availability, hormone levels, substrate availability and demand, and mitochondrial function. Metabolic flexibility is important for ensuring a continuous energy supply for use by the heart, and for providing optimal use of oxygen to produce ATP. Therefore, systemic conditions affecting substrate availability and/or uptake will impact cardiac metabolic flexibility, ultimately affecting cardiac function. For example, perfusates from isolated working hearts of diabetic *db*/*db* mice revealed a reduction of glucose oxidation by 52% and an increase in palmitate oxidation by 29% compared to controls[86,]. These diabetic animals were shown to display increased LV end diastolic pressures, a reduction in cardiac output, and a significant reduction in cardiac power, suggesting early signs of diabetic cardiac disease or DCM[86]. Furthermore, increasing infused palmitate levels stimulated an increase in myocardial oxygen consumption, which suggests increased fatty acid usage by the tissue[25]. Since FAO is less efficient than aerobic glucose oxidation (requiring higher mitochondrial oxygen consumption per ATP produced), this suggests that diabetic hearts operate under reduced metabolic efficiency, which puts diabetic hearts at a significant mechanical disadvantage[42].

T2DM induces specific changes to mitochondrial respiratory pathways, which in turn affects the ability of the heart to efficiently metabolize energy substrates. In general, the literature suggests that mitochondria exposed to conditions of DM are prone to dysfunction. Significant changes in mitochondrial activity, ADP-stimulated OXPHOS capacity,

biogenesis, protein expression and morphology have been reported in the skeletal muscle, hepatic tissue, and adipose tissue of insulin-resistant individuals[87]. Increased cellular and mitochondrial uptake of fatty acids in combination with increased FAO occurs in the diabetic heart, which may lead to ectopic lipid accumulation[88]. Defects to the OXPHOS capacities of the ETS Complexes I[80,84], II[82], and IV[80] have been reported in rodent models of T2DM. Poor coupling between substrate oxidation and phosphorylation has been shown in permeabilized atrial tissue of human T2DM patients, which is suggestive of mitochondrial uncoupling[41]. Furthermore, mitochondrial reactive oxygen species (ROS) are a significant contributor to oxidative stress associated with T2DM, and can be produced at CI, CIII, or during electron transfer from acyl dehydrogenases to ubiquinol during FAO[89,90]. Finally, fragmentation of the cardiac mitochondrial network has been reported in hepatic cell lines[91] and human atria[41] in response to hyperglycemic conditions. Reducing mitochondrial size may reduce capacity for oxidative phosphorylation. Morphological defects in cardiac mitochondria have also been shown to impair cardiac recovery post-MI in hearts of diabetic *ob/ob* mice, as indicated by reduced ejection fraction and poor animal survival rates[92]. These findings are indicative of reduced metabolic efficiency in the diabetic heart.

A.1.8 High Resolution Respirometry: Measurement of Integrated Mitochondrial Function

There is increasing interest in the monitoring of mitochondrial function and dysfunction *in vitro*, as mitochondria have been implicated in the pathophysiology of numerous disease processes. Consumption of oxygen by the process of OXHPOS can be measured using oxygen electrodes attached to a respiration chamber. As the process of OXPHOS occurs in the mitochondria from the biological sample, the oxygen added to the chamber is converted to water, and a resulting decrease in the oxygen concentration in the chamber is recorded[93]. Traditional respirometry assumes that samples exist in a closed

system, where consumption of oxygen occurs exclusively by metabolic reactions within the sample. Unfortunately, this is not the case, as oxygen flux should be corrected for oxygen back-diffusion and oxygen consumption by the polarographic oxygen sensors. Other limitations associated with traditional respirometry include low signal stability, high limits of detection (preventing ability to utilize small tissue samples), and limited titration steps due to low chamber volume. Due to the sensitive nature of functional mitochondrial testing, these older methods are now considered unreliable[94].

High-resolution respirometry (HRR, Oroboros Oxygraph 2k, O2k, Oroboros Instruments, Innsbruck, Austria)) has emerged as an advanced technique for investigating functional capacities of mitochondria *in vitro*. The term "high-resolution" refers to a limit of detection of oxygen flux as low as 1 pmol $O_2.s^{-1}.ml^{-1}$, allowing for measurements in very small samples without sacrificing measurement accuracy or sensitivity. Materials used to construct the O2k are specifically selected to minimize oxygen diffusion, and to improve the sensitivity of the electrode, thus increasing the signal to noise ratio. HRR allows evaluation of the capacity of mitochondrial complexes, enzymes, and transporters in real time, by detecting fluctuations in oxygen consumption in the presence of different substrates, uncouplers, and inhibitors. This enables detection of specific defects in the mitochondrial OXPHOS process[93]. The O2k is considered the gold standard in respirometry. Conceptualized in 1989, the O2k consists of twin oxygen sensors adjacent to Duran glass chambers with adjustable volume, encased in an insulated copper block[94]. The block is electronically and precisely controlled with a built-in Peltier thermostat Samples are separated from sensors by an oxygen-permeable 25 μm fluorinated ethylene propylene membrane.[95] Oxygen concentration is measured amperometrically by the Clark-type

polarographic oxygen sensors (OroBoPOS), which consist of a gold cathode and silver/silver chloride anode[95].

Another advantage of the O2k is the software DatLab (Oroboros Instruments, Innsbruck, Austria) which provides an online display of oxygen concentration and respiration (oxygen flux or negative derivative of oxygen concentration as a function of time) in real-time for each chamber. This allows the user to easily run multiple protocols simultaneously[95].

A.1.9 Animal Models of Type 2 Diabetes

An increasing number of experimental animal models are becoming available for the study of T2DM and its complications. Most involve the expression or suppression of key genes in lines that are genetically similar, allowing selection for traits of interest. For instance, the leptin-receptor deficient *db/db* mouse represents a useful monogenic model of obesity and T2DM; animals demonstrate elevated plasma insulin by as early as 10-12 days of age, and are nearly double the weight of control mice (40-50g compared to 25g) by as early as 2 months of age. Furthermore, these animals are useful for the study of cardiovascular diabetic complications independent of atherosclerotic and hypertensive factors, as *db/db* rodents are resistant to atherosclerosis and hypertension[96,97]. Therefore, cardiac complications can manifest free of underlying heart disease. The hearts of *db/db* mice mimic the marked metabolic inflexibilty manifested in humans, with a preferential use of fatty acid oxidation by cardiomyocytes as a source of energy over glycolytic and glucose oxidation sources, making them useful for investigating cardiac outcomes from dyslipidemia[86]. However, because the *db/db* model is an inbred transgenic model, it is difficult to know whether all complex pathogenic mechanisms present in humans are also present in each animal.

Experimentally induced animal models make use of non-genetically manipulated animal strains, which are more readily available, and considerably cheaper than transgenic models. Induction of T2DM is typically achieved using chemical or dietary means. As these animals mature, their health status resembles the pathogenesis of diabetes in humans. Rodent species, animal age, pre-treatment nutritional and health status, as well as route of administration (if applicable) must be carefully considered. Although there is no model that perfectly recapitulates T2DM progression, the majority of models do demonstrate some primary hallmarks of T2DM: hyperglycemia, insulin resistance, and/or subsequent beta-cell dysfunction. Experimental approaches used to induce T2DM include injections with streptozotocin (STZ) or alloxan, fructose feedings or other high sugar/fat alternatives, administration of monosodium glutamate (MSG) injections to intrauterine growth restricted (IUGR) animals, and various combinations thereof[96]. Alloxan models undergo selective pancreatic beta-cell loss by generation of oxidant species within the tissue; however, these models have steadily lost popularity due to alloxan's limited efficacy, and side effects affecting the liver and kidneys[98]. STZ models are more appealing, as manipulating dosage and time course of diabetogenic injections gives a phenotype of varying severity, with high dose STZ (> 60kg/mg body weight) causing massive beta cell destruction akin to T1DM, and multiple intermediate doses (~40-55 kg/mg body weight) producing an intermediate phenotype more characteristic of T2DM. STZ is a broad-spectrum antibiotic originally isolated from *Streptomyces achromogenes* that acts to inhibit DNA synthesis by alkylating DNA and subsequently poly-ribosylating ADP, thus depleting NAD^+ and ATP[99]. STZ-injected animals are consistently insulin-resistant after 9 days with high dose STZ, and will also develop hyperglycemia, hyperinsulinemia, and elevated serum free fatty acids/triglycerides by

approximately 4 months of age[69, 70]. These effects are exacerbated by high-fat feeding and often coincide with obesity[100].

Selection of the optimal model to study outcome parameters is crucial, as physiological attributes of each model may affect parameters of interest. As such, new models of T2DM are being introduced to the lab environment to model specific aspects of T2DM and related complications. Here, we present a promising candidate for the study T2DM, and its associated cardiac complications.

A.1.10 Nile Grass Rat model of Type 2 Diabetes

The Nile Grass rat *Arvicanthis niloticus* (NR) has recently emerged as a promising candidate model for studying protracted metabolic disease[101]. NRs are herbivorous murine rodents, native to sub-Saharan Africa[102]. These animals are comparable in size and weight to young rats, weighing approximately 90-120 g. Unlike common lab rodents, NRs display diurnal tendencies; this makes them a valuable model for the study of circadian rhythm[103] and neural activation[104]. Furthermore, the retina of the NR is cone-rich compared to the cone-poor retinas of other rodents, making them useful for the study of optic diseases known to occur in humans[105].

Recent studies have investigated the tendency of NRs to spontaneously develop pathological markers congruent to the Metabolic Syndrome (MetS) and T2DM progression in humans[101,106]. Noda *et al.* studied over 1100 NRs bred in captivity, from an initial group of 29 NR founders trapped in their native environment by Dr. Laura Smale[101]. Interestingly, they reported that chow-fed animals displayed dyslipidemia and hyperglycemia by one year of age[101]. Further investigation revealed other indicators of T2DM: liver steatosis, advanced-glycation endproduct (AGE) accumulation in renal tissue, disrupted islet cell distribution and morphology, elevated triglycerides (TGs), and persistent hyperinsulinemia at early stages of

disease progression. A strong correlation between elevated TGs and HbA1c was noted, suggesting that aberrant lipid metabolism in these animals may correlate with disease progression, as is seen in humans[101]. Work by our lab and others has shown that NRs develop hyperinsulinemia by as early as 2 months of age, and follow a predictable disease course, similar to that seen in humans[107]. The model of diabetes progression proposed by Weir *et al.* in 2004 suggests a framework for categorizing diabetes progression that corresponds to the metabolic decline of the NR[108]. Based on this model, normoglycemic NRs aged 2 months represent a subclinical stage 1 (Figure 1.1, compensation). Hyperglycemic NRs aged 6 months represent stage 2 (Figure 1.1, decompensation), and hyperglycemic NRs aged 18 months represent stage 4 or 5 (Figure 1.1, severe decompensation and collapse)[109]. To our knowledge, the Sauvé lab currently maintains the only laboratory colony of NRs in Canada, which have been utilized primarily to study vascular and retinal circuitry changes associated with diabetic retinopathy[110]. Studies on the cardiovascular status of these animals have not been attempted, and will provide valuable insight into cardiac changes occurring over time. Our preliminary findings do support that the NR model of T2DM exhibits hallmarks of cardiovascular dysfunction during their lifespan.

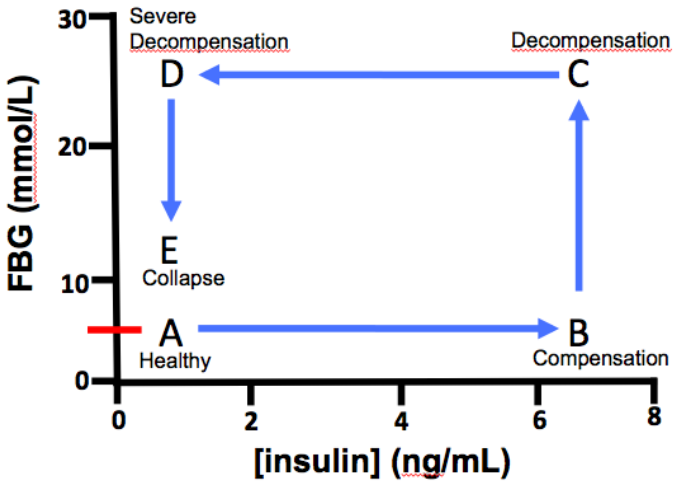

Figure 1.1 ***Progression of Type 2 Diabetes Mellitus in the Nile Grass Rat.*** Healthy NRs maintain a low fasted blood glucose (FBG) and plasma insulin (A). On a standard chow diet, hyperinsulinemia occurs at 2 months of age (B), which is followed by hyperglycemia at 6 months of age (C) and severe decompensation up to 18 months of age (D). Stage (E) is thought to occur in elderly NRs (18 months+), and represents complete metabolic collapse. Red line represents cut-off for hyperglycemia in NRs (FBG > 5 mmol/L).

A.2 Chapter 2 - EXPERIMENTAL RATIONALE

As approximately 1 in every 11 adults worldwide currently lives with diabetes, it is evident that holistic strategies are warranted to improve prevention and treatment approaches. A better understanding of the aetiology, pathophysiology, and symptom progression of T2DM may improve treatment efficacy, and elucidate alternative pathways of intervention. The NR model of T2DM provides a unique opportunity to study the onset of pathology free of induced pharmacological effects seen in other animal models. Cardiac studies in this animal model have not been undertaken. Furthermore, understanding of early indicators of dysfunction induced in pre-diabetic stages could hasten clinical intervention, and prevent the development of severe complications.

A.2.1 Hypothesis

We hypothesize that prodromal functional mitochondrial changes will be occurring in cardiac ventricular tissue, prior to the onset of clinically detectable hyperglycemia and/or hyperinsulinemia.

A.2.2 Aims

1. To evaluate the viability of the NR model of T2DM as a model of diabetic cardiac complications.
2. To investigate early changes in cardiac mitochondrial function using high-resolution respirometry.
3. To examine differential effects of diet, and age on cardiac mitochondrial function.
4. Provide preliminary echocardiographic data on the cardiac function of the healthy and diabetic NR.

A.3 Chapter 3 - METHODS

A.3.1 Experimental Animal Model

Male NRs were maintained on a 14:10 h light-dark cycle, at room temperature of 21±2 °C and relative humidity of ~40 %. After weaning at 21-23 days, the animals were divided into two dietary groups. The control group was fed a high-fiber diet (Mazuri® Chinchilla Diet, 5M01, Purina Mills, LLC, St. Louis, MO, USA; 4.0 % fat, 15.3 % fibers, 21.6% protein). The diabetic group was fed standard rodent chow (Prolab® RMH 2000, 5P06, LabDiet, Nutrition Intl., Richmond, IN, USA; 9.6 % fat, 3.2 % fibers, 19.9 % protein). Nutritional information for the Prolab and Mazuri diets are presented in Table 1. The animals received food and water *ad libitum*. A fasting period of 16-18 hours preceded blood and tissue collection, but did not precede electrocardiography. Animals were studied at 2, 6, 12 (echo only) or 18 months of age. All experiments were carried out in accordance with the Institutional Animal Care and Use Committee (University of Alberta) and the NIH (USA) guidelines regarding the care and use of animals for experimental procedures.

Table 3.1 Nutritional content of Prolab and Mazuri diets.

Mazuri® Chinchilla Diet

Nutrients	
Protein, %	**20**
Arginine, %	1.2
Cystine, %	0.28
Histidine, %	0.49
Isoleucine, %	1.1
Leucine, %	1.5
Lysine, %	1.1
Methionine, %	0.53
Phenylalanine, %	1.0
Tyrosine, %	0.67
Threonine, %	0.80
Tryptophan, %	0.28
Valine, %	1.0
Fat (Ether extract), %	**4.1**
Linoleic Acid, %	1.6
Fiber (Crude), %	**15**
Neutral Detergent Fiber, %	29
Acid Detergent Fiber, %	17
Starch, %	9.8
Glucose, %	0.21
Fructose, %	0.75
Sucrose, %	2.61
Lactose, %	0.56
Metabolizable Energy, kcal/kg	2,910

Minerals	
Ash, %	6.9
Calcium, %	0.90
Phosphorus, %	0.67
Potassium, %	1.7
Magnesium, %	0.3
Sodium, %	0.26
Chloride, %	0.55
Iron, ppm	350
Zinc, ppm	119
Manganese, ppm	95
Copper, ppm	15
Iodine, ppm	0.87
Selenium, ppm	0.30
Cobalt, ppm	1.2

Vitamins	
Thiamin, ppm	4.9
Riboflavin, ppm	5.6
Niacin, ppm	48
Pantothenic acid, ppm	19
Choline, ppm	1,710
Folic acid, ppm	9.8
Pyridoxine, ppm	7.6
Biotin, ppm	0.25
Vitamin B_{12}, µg/kg	12
Vitamin A, IU/kg	33,440
Vitamin D_3, IU/kg	1,780
Vitamin E, IU/kg	230
Vitamin K, ppm	2.7
Beta-carotene, ppm	15

Prolab® RMH 2000

Nutrients	
Protein, %	**19.9**
Arginine, %	1.10
Cystine, %	0.27
Glycine, %	1.12
Histidine, %	0.43
Isoleucine, %	0.92
Leucine, %	1.45
Lysine, %	1.03
Methionine, %	0.33
Phenylalanine, %	0.82
Tyrosine, %	0.52
Threonine, %	0.72
Tryptophan, %	0.25
Valine, %	0.98
Serine, %	0.98
Aspartic Acid, %	1.78
Glutamic Acid, %	4.68
Alanine, %	0.93
Proline, %	1.66
Taurine, %	0.01
Fat (Ether extract), %	**9.6**
Cholesterol, ppm	78
Linoleic Acid, %	4.93
Linolenic Acid, %	0.70
Omega-3 Fatty Acids, %	0.76
Fiber (Crude), %	**3.2**
Neutral Detergent Fiber, %	12.3
Acid Detergent Fiber, %	4.4
Starch, %	25.7
Glucose, %	0.0
Fructose, %	0.1
Sucrose, %	0.6
Lactose, %	9.0
Metabolizable Energy, kcal/kg	3,520

Minerals	
Ash, %	6.5
Calcium, %	0.80
Phosphorus, %	0.81
Potassium, %	1.08
Magnesium, %	0.23
Sodium, %	0.48
Chloride, %	0.75
Iron, ppm	440
Zinc, ppm	150
Manganese, ppm	120
Copper, ppm	15
Iodine, ppm	1.4
Selenium, ppm	0.14
Cobalt, ppm	0.37

Vitamins	
Thiamin, ppm	7.9
Riboflavin, ppm	12
Niacin, ppm	54
Pantothenic acid, ppm	16
Choline, ppm	1,800
Folic acid, ppm	0.90
Pyridoxine, ppm	5.4
Biotin, ppm	0.29
Vitamin B_{12}, µg/kg	15
Vitamin A, IU/kg	19,000
Vitamin D_3, IU/kg	1,500
Vitamin E, IU/kg	49
Vitamin K, ppm	1.3
Beta-carotene, ppm	2.0

Animals were fed *ad libitum* for the duration of the study period. The Mazuri diet contains higher fibre and lower fat, whereas the Prolab diet is considered standard rat chow[107].

A.3.2 Echocardiographic In vivo Functional Assessment

Thoracic echocardiography was performed on 12 month of age NRs (5 Prolab-fed, 4 Mazuri-fed) according to a slightly modified procedure[111,112]. NRs were mildly anaesthetized (sedated with 3 % isoflurane and maintained with 2% isoflurane) using a nosecone (VEVO Compact Anaesthesia system). Anaesthesia was monitored every 5 minutes using physiological measures (ECG display, heart rate, respiratory rate) and maintained for ~30 min per animal. NRs body temperature was monitored using a rectal probe and a warmed platform (P/N 11437 VisualSonics™) was used to maintain optimal physiological temperature at 37 °C. Animal paws were taped to ECG metal strips on the same platform to record ECG tracings simultaneously with imaging. Hearts were imaged using the Vevo 770™ High-Resolution In-Vivo Micro-Imaging System (Fujifilm VisualSonics Inc.) and a 17.5 MHz Scanhead probe for high-frequency ultrasound imaging. The upper anterior chest (superior to the xyphoid process) was shaved using an electric shaver, and then fine hair was removed using Nair® depilatory cream. Warmed ultrasound gel was applied immediately prior to imaging. Ventricular dimensions were measured using M-mode transthoracic echocardiography at the level of the papillary muscles, imaging a minimum of 3 cardiac cycles. Percent ejection fraction and fractional shortening were calculated from M-mode images. Doppler tissue imaging from the apical four chamber view was used to assess mitral valve annular velocities, E' and A'. In addition, pulse wave Doppler of the mitral E and A wave velocities were taken from the four chamber view. The isovolumic relaxation time (IVRT), isovolumic contraction time (IVCT) and aortic ejection time (ET) were measured from these waveforms to determine myocardial performance index. The myocardial performance (Tei) index was calculated using the equation (IVRT+ IVCT)/ET[111]. Blood pressure measurements were not recorded.

A.3.3 Fasted Blood Glucose, Plasma Insulin, and Glycated Hemoglobin A1c

After overnight fasting, a tail blood sample was taken to measure fasting blood glucose (FBG) using a scalpel and an Accu-chek Compact Plus glucose monitoring system (Roche, Mississauga, ON, Canada). A value of FBG >5.0 mmol l^{-1} is considered hyperglycemic, based on previous work on NRs by our lab[107,110].

NRs were then euthanized with an intra-peritoneal injection of a lethal dose (480 mg kg^{-1}) of pentbarbitol sodium (Euthanyl Bimeda-MTC Animal Health Inc., Cambridge, ON, Canada). Following establishment of surgical plane, the blood was collected through cardiac puncture and transferred into a K_2-EDTA-coated BD Microtainer™ tube with Microgard™ closure (Becton, Dickinson and Company, Mississauga, ON, Canada). The blood was immediately centrifuged at 2000 rpm for 20 minutes at 4 °C. The plasma was collected and stored at -80 C until later use to determine insulin and glycated hemoglobin (HbA1c) levels.

The insulin level was measured using an insulin ELISA kit (Ultra Sensitive Mouse Insulin ELISA kit #90080. Crystal Chem Inc., Downers Grove, IL, USA). A fasting insulin level over 2 ng ml^{-1} was considered indicative of compensation[1].

HbA1c level in frozen hematocrit samples was determined using a modified ELISA kit according to manufacturer's instructions [Crystal Chem Inc (Downers Grove, IL) Mouse Hemoglobin A1c Assay #80310, Mouse HbA1c Controls #80313]. Samples were thawed on ice prior to use, mixed using gentle agitation and the assay was performed in duplicate for each sample. Absorbance was measured using a BioTek™ Synergy™ Mx Multimode Microplate Reader on Costar3596 96-well plates, at an absorbance of 700 nm. Variation of absorbance was calculated using the following formula:

$$\Delta A = (OD_{700\ nm,\ 180\ sec}) - (OD_{700\ nm,\ 0\ sec}) \times 185/255$$

Sample concentrations were interpolated using the linear equation of absorbance variation on the y axis versus HbA1c concentration (%HbA1c) on the x axis. As HbA1c % cutoffs vary among animal models, the HbA1c% cutoff was set at 6% (average of Mazuri-fed animals, independent of age, plus two times the standard deviation).

A.3.4 Cardiac Tissue Collection and Permeabilized Fibre Preparation

Whole hearts were collected from euthanized animals. The heart was immediately immersed in ice-cold BIOPS relaxing buffer (in mM; 2.77 CaK_2EGTA, 7.23 K_2EGTA, 20 immidazole, 20 taurine, 6.56 $MgCl_2$, 5.77 ATP, 3.95 phosphocreatine, 0.5 dithiothreitol, 50 K-MES, pH 7.1 at 0 °C)[113,114]. Superior cardiac structures (aorta, pulmonary artery, upper atria) were immediately removed, approximately 30 mg of left ventricular tissue was isolated at the apex for fiber preparation, and the remaining cardiac tissue was immediately frozen at -80 C for future immunoblotting and aconitase assays. The apex was transferred into fresh ice-cold BIOPS solution and kept on ice at all times. The left ventricular tissue was manually dissected with forceps and the resulting fibre bundles were permeabilized by gentle agitation for 30 min at 4 °C in relaxing buffer supplemented with 50 μg ml^{-1} saponin [113,114,115]. Fibres were washed for 10 min by agitation in ice-cold mitochondrial respiration medium MiR05 containing 110 mM sucrose, 60 mM K-lactobionate, 0.5 mM EGTA, 1 g l^{-1} bovine serum albumin fatty acid free, 3 mM $MgCl_2$, 20 mM taurine, 10 mM KH_2PO_4, and 20 mM K-N-2hydroxyethylpiperazine-N-2-ethanesulponate (HEPES) (pH 7.1)[116]. The fibers were then blotted, weighted and immediately used for respirometric measurements. The remaining cardiac tissue was immediately frozen at -80°C for future immunoblotting and aconitase assays.

A.3.5 High Resolution Respirometry on Permeabilized Cardiac Fibres

Respiration was measured at 37 °C using the Oroboros Oxygraph-2K (Oroboros Instruments, Innsbruck, Austria). Protocols were run using 2.0 – 4.5 mg permeabilized ventricular fibres in each chamber containing 2 ml of MiR05. Oxygen diffusion limitation of flux was avoided by maintaining oxygen levels at over 200 μM O_2[117]. Datlab software (Orobotos Instruments, Innsbruck, Austria) was used for data acquisition and analysis. Instrumental background flux was calibrated as a function of oxygen concentration and substracted from the total volume-specific oxygen flux[118–120]. Four protocols were applied to the permeabilized fibers, including two states: (1) LEAK respiration measuring the non-phosphorylated state in the absence of ADP, and (2) OXPHOS capacity measuring the oxygen consumption coupled to phosphorylation of ADP to ATP in the presence of saturating ADP. The different substrate combinations included for the evaluation of OXPHOS capacity (in the presence of saturating ADP and cytochrome *c*) and the related pathways, complexes, enzymes, and transporters are presented in Table 2.

Table 3.2 Evaluation of mitochondrial oxidative phosphorylation (OXPHOS) in the presence of different substrate combinations, and the related pathways and specific steps targeted by the measurement.

Protocols	**Substrate combinations (with saturating ADP and cytochrome *c*)**	**Pathways**	**Specific complexes, enzymes, and transporters measured**
1	Pyruvate+malate (PM)	NADH	Complex I Pyruvate dehydrogenase complex Pyruvate transporter
1	Pyruvate+malate+succinate (PMS)	NADH & Succinate	Complexes I & II Pyruvate dehydrogenase complex Pyruvate transporter Succinate dehydrogenase
1	Succinate+rotenone (after PM)	Succinate	Complex II Succinate dehydrogenase
1	Ascorbate+TMPD(-azide-background)		Complex IV single step
2	Palmitoylcarnitine+malate	ETF	Long chain fatty acid oxidation Carnitine translocase Carnitine palmitoyltransferase-II
3	Octanoylcarnitine+malate	ETF	Medium chain fatty acid oxidation Carnitine translocase Carnitine palmitoyltransferase-II
4	Acetylcarnitine+malate	ETF	Carnitine acetyltransferase Carnitine translocase

Abbreviations: ETF, electron transferring flavoprotein; TMPD, N,N,N,N-tetramethyl-p-phenylenediamine.

In the first protocol, the following substrates and inhibitors were added sequentially (final concentration in the chamber shown): pyruvate (5 mM), malate (5 mM), ADP (2.5 mM), cytochrome *c* (10 μM), succinate (10 mM), rotenone (1 μM), antimycin A (5 μM), ascorbate (2 mM), tetramethylphenylenediamine (TMPD; 0.5 mM), and sodium azide (100 mM). A variation of this protocol including the addition of the uncoupler dinitrophenol (DNP) was performed in early experiments on a reduced number of animals to confirm no limitation of the OXPHOS capacity by the phosphorylation system in the NR heart. This first standard protocol measured the LEAK respiration (before the addition of ADP), the NADH pathway capacity (flux through complex I, in the presence of pyruvate+malate and ADP), the NADH & succinate pathways capacity (convergent electron flux through complex I&II in the presence of pyruvate+malate+succinate and ADP), the succinate pathway capacity (electron flux through complex II after inhibition of complex I with rotenone), and the complex IV single step activity (with ascorbate+TMPD, after subtraction of the background in the presence of azide).

The three remaining protocols (2, 3, and 4; see Table 1) involved FAs as substrates to evaluate β-oxidation. Three different combination of substrates were used, including the long chain FA palmitoylcarnitine (+malate), the medium chain FA octanoylcarnitine (+malate), and acetylcarnitine (+malate). LEAK respiration was first measured in the presence of the FA substrate and malate, without ADP. Then ADP and cytochrome c were added to measure OXPHOS capacity. The order of protocols (standard versus β-oxidation) were rotated to account for time permeabilized fibres spent on ice between protocols.

At the end of each experimental run, the chamber contents were removed and chambers were rinsed twice with 500 μl of MiR05. The fibers were homogenized on ice for 2

times 30 s on ice with glass potters and immediately stored at -80 °C for measurement of citrate synthase.

A.3.5.1 Metabolic Substrates

High resolution respirometry protocols are designed to target specific respiratory states of the ETS, which allows for evaluation of mitochondrial function. Metabolic substrates used in HRR protocols are administered sequentially to experimentally reconstitute integrity of metabolic mitochondrial pathways, which use a combination of enzymes, protein complexes, and substrates to function. The breakdown of substrates ensures delivery of reducing equivalents to the ETS, which drives electron flux to CIV, and conversion of terminal oxygen to water in conjunction with ATP synthesis.

Pyruvate+Malate (PM): Addition of PM supplies the NADH pathway, so named because it activates dehydrogenases through reduction of NAD+ into NADH. It consists of the pyruvate carrier, the pyruvate dehydrogenase complex (PDC), and electron flow through CI, among others. Pyruvate is transported into the mitochondrial matrix by the pyruvate carrier, where it is converted to acetyl-CoA by the PDC. Upon addition of malate, citrate synthase enzymatically condenses oxaloacetate with acetyl-CoA to generate citrate. High added malate necessitates equilibration with fumarate, and fumarate rises. The increase in fumarate inhibits electron flux from succinate to fumarate, and the formation of flavin adenine dinucleotide ($FADH_2$). Furthermore, oxaloacetate produced by oxidation of malate inhibits CII (succinate dehydrogenase). Taken together, addition of PM ensures flux of electrons from NADH through CI, but not CII[69].

Pyruvate + Malate + Succinate (PMS): Addition of succinate to the NADH pathway substrates for CI (here PM) supports additional electron flow through CII via

$FADH_2$. Thus, PMS evaluates convergent electron flow through NADH (CI) and Succinate (CII) pathways[69].

Succinate (Rotenone) [S(Rot)]: Addition of rotenone inhibits electron flux through CI. Electron flux through CII from succinate via $FADH_2$ continues, meaning that S(Rot) protocol evaluates electron flux through the Succinate pathway alone, without contribution from CI.

Ascorbate + TMPD (AsTm): TMPD is administered as a non-physiological substrate to reduce cytochrome *c*, and thus measure the electron flow through CIV. Ascorbate is administered first to maintain TMPD in a reduced state[121].

AcetylCarnitine (AcetylCar): AcetylCar is translocated into the mitochondrial matrix by carnitine translocase, and then converted to acetyl-CoA by carnitine acetyltransferase.

Octanoylcarnitine (OctCar): OctCar is a medium-chain fatty acid (8C). OctCar is provided in the presence of malate, and enters the mitochondrial matrix using carnitine translocase. It is converted to octanoyl-CoA by carnitine palmitoyltransferase II (CPTII) and then undergoes medium-chain FAO to produce acetyl-CoA[122].

Palmitoylcarnitine (PalCar): Palmitoylcarnitine is a long-chain fatty acid (16C) that enters the mitochondrial matrix using carnitine translocase. It is then converted to palmitoyl-CoA by carnitine palmitoyltransferase II (CPTII), and then undergoes long-chain FAO to produce acetyl-CoA[122].

Malate was added to each fatty acid protocol to stimulate the entry of acetyl-CoA into the TCA cycle and favor the entry of electrons through CI[117,123].

A.3.6 Citrate Synthase Enzymatic Activity Assay

Citrate synthase activity is a well-accepted method for measuring mitochondrial content within samples[124,125]. Citrate synthase (CS) activity was measured at 37 °C, according to a previously described method, with slight modification to adapt it for a reading on a BioTek™ Synergy™ Mx Multimode Microplate Reader[126]. The absorbance was measured at 412 nm following the reduction of 0.1 mM 5,5' dithiobis-2-nitrobenzoic acid (ε 13.6 mL cm^{-1} μmol^{-1}) in the presence of 0.31 mM acetyl-CoA, 0.5 mM oxaloacetic acid, 0.25 % triton X-100, and 100 mM Tris-HCl buffer (pH 8.1). Five µl of the homogenate was added to wells immediately prior to reading 6 wells at a time for 3 minutes and 20 seconds. CS activity was expressed in International Units (IU) per mg of fibers, where IU is one µmol of substrate transformed per min and 20 seconds[125].

A.3.7 Data Analysis

Statistical analyses were performed with SigmaPlot 14 (Systat Sofware Inc., San Jose, CA, USA). Graphics were produced using GraphPad Prism 7 (GraphPad Software, Inc., La Jolla California). For data of mitochondrial function, the criteria of normality and homogeneity of variance for ANOVA were tested for each variable using Kolmogorov-Smirnov (Lilliefor's correction) and Brown-Forsythe tests, respectively. Two variables were transformed to meet the criteria: LN transformation for Octanoylcarnitine+malate OXPHOS capacity and square root transformation for CS activity. Two-way ANOVA was applied to test the effect of diet and aging on mitochondrial function data, followed by pairwise Tukey's tests. Two of the variables in FCR (Complex IV and LEAK for the NADH pathway) did not meet the criteria with any transformation and were analysed using Kruskall-Wallis one-way ANOVA on rank. Data are presented without transformation. A $p<0.05$ was considered significant. For metabolic data (fasting blood glucose, plasma insulin, body

weight, HbA1c), Mann-Whitney U-test was applied to test the effect of diet on metabolic parameters. Data are presented as median (min-max). A $p<0.05$ was considered significant.

Echocardiographic images were analyzed using Vevo LAB MX250 software (©2017 FUJIFILM VisualSonics Inc.), and statistical analyses were performed with SigmaPlot 14 (Systat Sofware Inc., San Jose, CA, USA). Mann-Whitney U-test was applied to test the effect of diet on echocardiographic parameters. All findings were normalized by animal body weight. Data are presented as median (min-max). A $p<0.05$ was considered significant.

A.4 Chapter 4 – RESULTS

A.4.1 Electrocardiographic In vivo Functional Assessment

Animals underwent full echocardiographic assessment to investigate cardiac function at 12 months. A summary of echocardiographic findings and general animal characteristics is presented in Table 4.1. Only parameters applicable to diastolic dysfunction and left ventricular hypertrophic changes are presented, as these are the most common early functional changes that occur in T2DM. There were no significant differences in blood glucose ($p = 0.857$), body weight ($p = 0.730$), or heart rate ($p = 0.111$) between Prolab and Mazuri-fed animals that underwent echo. Blood pressures were not recorded at the time of echo. M-mode measurements of LV dimensions showed no statistically significant differences in the left ventricular interventricular septum in diastole (IVSd) ($p = 0.556$), the left ventricular internal diameter in diastole (LVId) ($p = 0.556$), or the left ventricular posterior wall diameter in diastole (LVPWd) $p = 0.191$). Left ventricular ejection fraction (%) and fractional shortening (%) were also measured as indices of systolic function, and showed no significant differences between dietary groups (EF% $p = 0.730$, FS% $p = 0.556$)

Mitral inflow parameters including mitral E-wave and A-wave velocities (mm/s), mitral E/A ratio, isovolumetric relaxation time (IVRT, ms), and the Tei index of global systolic and diastolic myocardial performance were measured, and no significant differences in mitral inflow parameters between dietary groups were observed (E-wave $p = 0.905$, A-wave $p = 0.730$, E/A $p = 0.905$, IVRT $p = 0.286$, Tei index $p = 0.413$).

Mitral tissue Doppler E'-wave, A'-wave, and E/E' ratio were measured to investigate early indices of diastolic dysfunction. Of the animals that underwent echocardiography, 80% of Prolab animals had E'-waves that were slower than the A' wave, which is an indicator of early diastolic dysfunction. Supporting this finding, the E'-wave velocity showed a trend for a

reduction in Prolab animals compared to controls ($p = 0.0635$). Also in support of this finding, the E'/A' ratio was significantly reduced in Prolab-fed animals compared to controls ($p = 0.0159$). The E/E' ratio (an estimate of left ventricular filling, and key marker of ventricular diastolic function) showed a trend for an increase in Prolab-fed animals compared to controls (Mazuri 21.9(18.3-27.5), Prolab 28.5(23.0-34.1), $p = 0.0635$). There was no significant difference in A'-wave velocities between groups ($p = 0.905$).

Table 4.1. Comparison of general and echocardiographic parameters in Prolab and Mazuri-fed animals at 12 months of age.

Parameters	Prolab	Mazuri	p-value
Metabolic parameters			
Body weight (g)	107 (101-126)	109 (106-121)	0.730
Blood glucose (mmol/l)	3.7 (2.8-6.4)	3.4 (3.3-3.8)	0.857
Electrocardiography parameters			
Heart Rate (bpm)	469 (436-519)	395 (382-450)	0.111
IVSd (mm)	1.50 (1.20-1.70)	1.34 (0.94-1.37)	0.556
LVPWd (mm)	1.40 (1.20-1.60)	1.32 (1.00-1.39)	0.1905
LVIDd (mm)	3.48 (2.60-4.47)	4.05 (3.15-4.50)	0.556
Ejection Fraction (%)	75.4 (61.1-85.5)	79.3 (69.8-91.7)	0.7302
Fractional Shortening (%)	43.9 (32.5-53.2)	48.3 (38.9-62.8)	0.556
IVRT (ms)	22.2 (19.5-28.5)	27.8 (23.1-31.3)	0.286
E-wave (mm/s)	715 (510-930)	701 (632-746)	0.905
A-wave (mm/s)	527 (305-668)	451 (381-525)	0.730
E/A	1.39 (1.15-1.68)	1.53 (1.33-1.80)	0.905
Tei Index	0.774 (0.716-0.839)	0.764 (0.679-0.803)	0.413
E'-wave (mm/s)	24.6 (22.2-28.7)	32.3 (25.0-34.6)	0.0635
A'-wave (mm/s)	27.8 (21.3-32.8)	28.0 (22.3-31.9)	0.905
E'/A'	**0.890** (0.750-1.18)	**1.16** (1.09-1.19)	**0.016***
E/E'	28.5 (23.0-34.1)	21.9 (18.3-27.5)	0.0635

Data were normalized by body weight, and are presented as median (min-max). Mann-Whitney U-test was applied. *$p<0.05$.

A.4.2 Metabolic Profile

A.4.2.1 Dietary Effect on Fasted Blood Glucose

Fasted blood glucose (FBG) was measured to assess glycemic status (Figure 4.1.). Mazuri-fed NRs did not develop hyperglycemia at any age (2 months 2.70(2.20-3.90) mmol/L (n = 5), 6 months 3.25(2.40-3.70) mmol/L (n = 8), 18 months 3.2(2.40-4.50) mmol/L (n = 4)), establishing the Mazuri diet as a valid control for hyperglycemia (Figure 4.1). Consistent with previous work by our lab and others, NRs fed a standard chow diet were more susceptible to spontaneously developing hyperglycemia[101,106]. Hyperglycemia (FBG ≥ 5.0 mmol/L) was not detectable in Prolab-fed animals at 2 months (3.00(1.8-3.8) mmol/L (n = 4)) however, hyperglycemia was detected in 67% of Prolab-fed animals at 6 months (5.15(3.60-24.1) mmol/L (n = 6)) and 78% of Prolab-fed animals at 18 months (6.00(2.6-26.4) mmol/L (n = 9)). FBG values of Prolab-fed animals were significantly increased at 6 months ($p = 0.004$) and 18 months ($p = 0.0182$), when compared to age-matched controls.

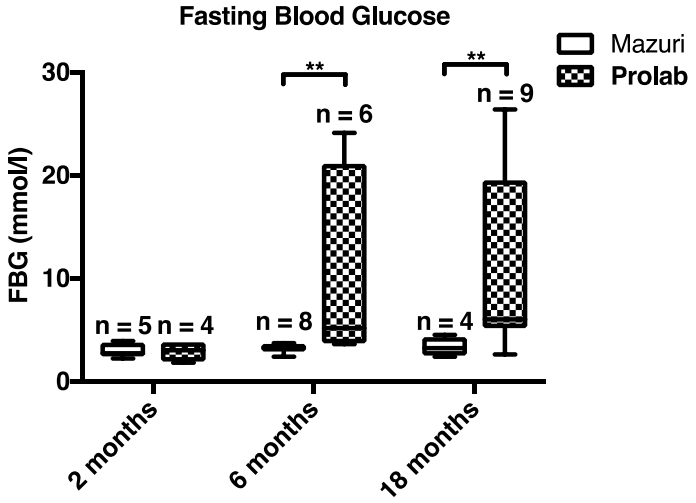

Figure 4.1. ***Dietary and aging effect on NR fasting blood glucose.*** Box and whisker plots of fasting blood glucose at 2 months, 6 months, and 18 months. Box plots show minimum, 25th percentile, median, 75th percentile, and maximum. Animals were considered hyperglycemic with FBG > 5.0 mmol/L. Mann-Whitney U-test was applied, **$p<0.01$, n = 4-9. Mazuri-fed animals maintained normoglycemia at all timepoints, whereas FBG was significantly increased in Prolab-fed animals at 6 and 18 months.

A.4.2.2 Dietary Effect on Body Weight

Consistent with previous work by our lab, Prolab-fed animals had increased body weights compared to age and sex-matched controls. Body weight was significantly increased in Prolab-fed animals at 6 months (110(108-120) g (n = 5), p = 0.0025) and 18 months (117(109-133) g (n = 8), p = 0.0121) compared to Mazuri animals (6 months 86.0(80.8-103) g (n = 7); 18 months 106(92.6-112)g (n = 4)).

A.4.2.3 Dietary Effect on Plasma Insulin

To further characterize the metabolic condition of the NRs, circulating plasma insulin was tested (Figure 4.2). Consistent with previous work in our lab, Mazuri animals exhibited a gradual increase in plasma insulin levels with age (2 months 0.582(0.325-1.70) ng/mL, 6 months 0.684(0.518-3.25) ng/mL, 18 months 2.49(1.16-3.23) ng/mL) (Figure 2.). Plasma insulin levels trended higher in Prolab-fed animals. Prolab-fed NRs exhibited a decrease in circulating plasma insulin from 2 months (6.19(1.20-10.0) ng/mL) to 6 months (4.26(1.04-5.60) ng/mL), followed by an increase at 18 months (5.74(2.59-8.61) ng/mL); however, these changes were not statistically significant. Aging did not significantly affect the plasma insulin level in either dietary group.

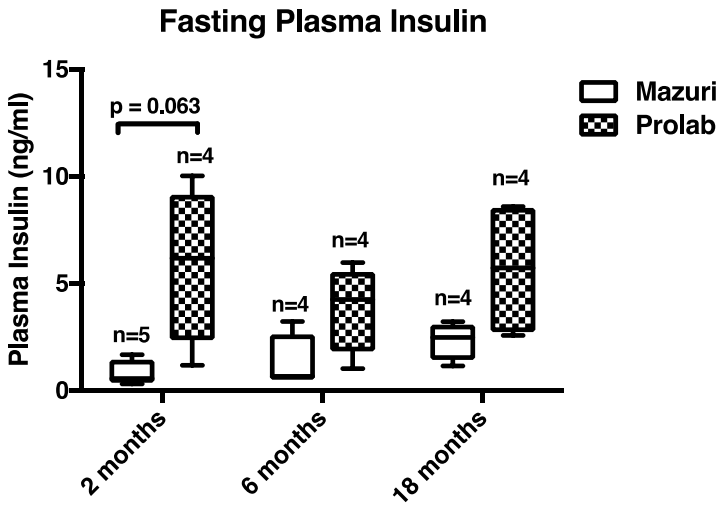

Figure 4.2. ***Dietary and aging effect on NR fasting plasma insulin.*** Box and whisker plot of fasting plasma insulin at 2 months, 6 months, and 18 months**.** Box plots show minimum, 25th percentile, median, 75th percentile, and maximum. Samples were tested in triplicate. Data were analyzed using Mann-Whitney U-test. *$p<0.05$, n = 4-5. Plasma insulin levels trended higher in Prolab-fed animals at all time points.

A.4.2.3 Dietary Effect on HbA1c

Concurrent with our FBG findings, %HbA1c was significantly increased in Prolab-fed animals at 6 months of age compared to age-matched controls, suggestive of hyperglycemia at this timepoint (Prolab 10.2(7.05-11.59) %, Mazuri 5.24(5.00-5.84) %, p = 0.0159) (Figure 4.3.). There was no significant dietary effect on % HbA1c at 2 months or 18 months; however, 75% of all Prolab animals were found to have HbA1c readings >6%. There were no statistically significant increases in %HbA1c in Mazuri or Prolab-fed NRs with aging.

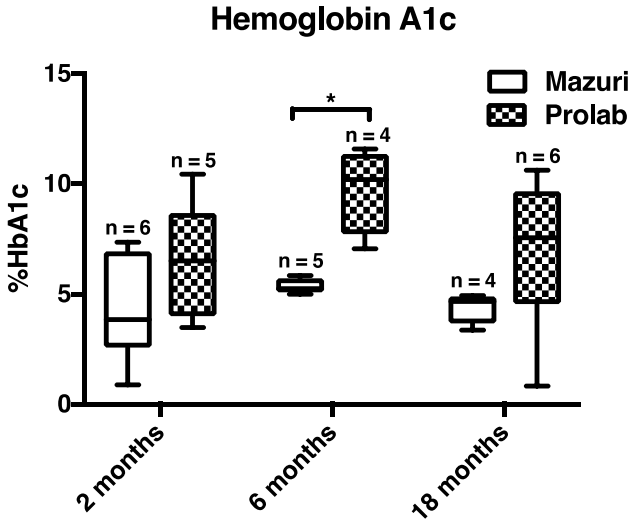

Figure 4.3. ***Dietary and aging effect on glycated hemoglobin A1c.*** Box and whisker plot of %HbA1c at 2 months, 6 months, and 18 months**.** Box plots show minimum, 25th percentile, median, 75th percentile, and maximum. Samples were tested in duplicate. %HbA1c > 6.0% was considered elevated. Data were analyzed using Mann-Whitney U-test. *p<0.05, n = 4-6. %HbA1c was significantly increased in Prolab-fed animals at 6 months compared to age-matched controls.

A.4.3 Cardiac mitochondrial function

A.4.3.1 Mitochondrial coupling and membrane integrity

The values of LEAK respiration in the presence of NADH-linked substrates pyruvate+malate were used to evaluate mitochondrial coupling. LEAK capacity expressed in flux per mg fibers did not vary between diets, at any of the age point (Fig. 4.4A). Aging from 2 to 6 months caused a significant decline in LEAK in the Prolab-fed animals ($p = 0.007$), indicating an increase in mitochondrial coupling.

LEAK respiration expressed as FCR indicates the coupling independent of mitochondrial content. The changes of FCR for LEAK indicated an increase in coupling (decrease in FCR for LEAK) from 2 to 6 months in the Prolab-fed animals (Kruskal Wallis, $p = 0.011$), followed by a decrease in coupling at 18 months of age (Kruskal Wallis, $p = 0.038$; Figure 4.4B.). These changes with age in the Prolab-fed animals lead to significant differences between diets at 6 and 18 months. At 6 months, Prolab-fed animals demonstrated better coupling compared to Mazuri-fed animals ($p = 0.016$). However, at 18 months of age, this difference is reversed with higher coupling in the Mazuri-fed animals ($p = 0.035$).

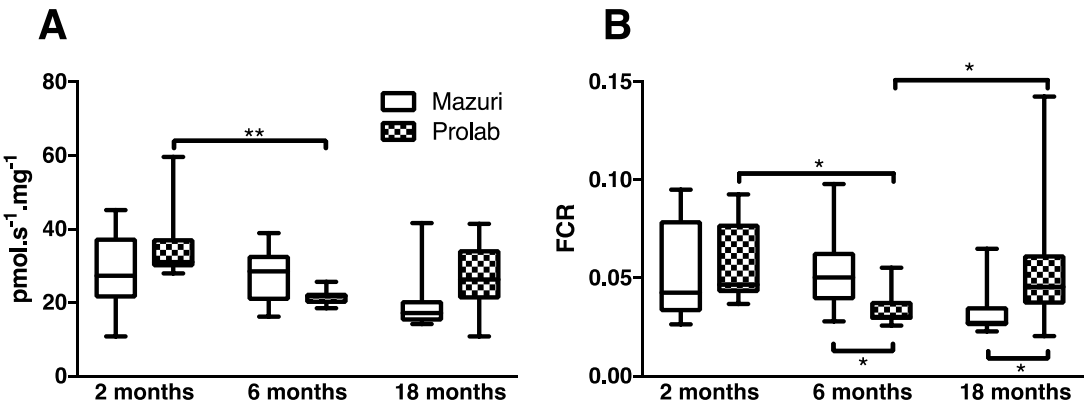

Figure 4.4. ***Dietary and aging effect on mitochondrial NADH pathway LEAK capacity.*** LEAK respiration was determined in the presence of substrates, and absence of ADP and ATP. Data are presented as box and whisker plots showing (A) flux/mass (pmol.s^{-1}.mg^{-1} wet weight) and (B) flux control ratio at 2 months, 6 months, and 18 months. Flux/mass data underwent cube root transformation to meet assumptions for two-way ANOVA. Aging effect on FCR was tested using One-way ANOVA. Kruskal-Wallis one-way analysis of variance was applied to test dietary effect on FCR data, without transformation. *$p<0.05$, **$p<0.01$ n = 7-12.

A slight increase in respiration due to cytochrome *c* addition after ADP was observed, indicating control of respiration by exogenous cytochrome *c*[69] (Figure 4.5). A value of 1.0 indicates no control of respiration by external cytochrome *c*, and thus full integrity of the outer mitochondrial membrane. All values except for one (Prolab group at 2 months) were within range of 0.85 to 1.00. This is a similar outer membrane integrity finding as reported previously with permeabilized fibers from human heart[113], rat heart[116,127], and mouse heart[114]. These results indicate good integrity of the mitochondrial membrane in the fiber preparation. There were some changes in mitochondrial outer membrane integrity occurring with diet or age. Age affected the Prolab-fed animals, showing a decrease in mitochondrial integrity from 2 to 18 months ($p = 0.027$), and an increase from 6 to 18 months ($p = 0.003$). The difference in membrane integrity between the dietary groups was significant only at 6 months, with a decrease in integrity in the Prolab-fed animals ($p < 0.001$). In order to not have all results accounted for in these differences in membrane fragility, we accounted for externally added cytochrome *c* in all the results for OXPHOS values.

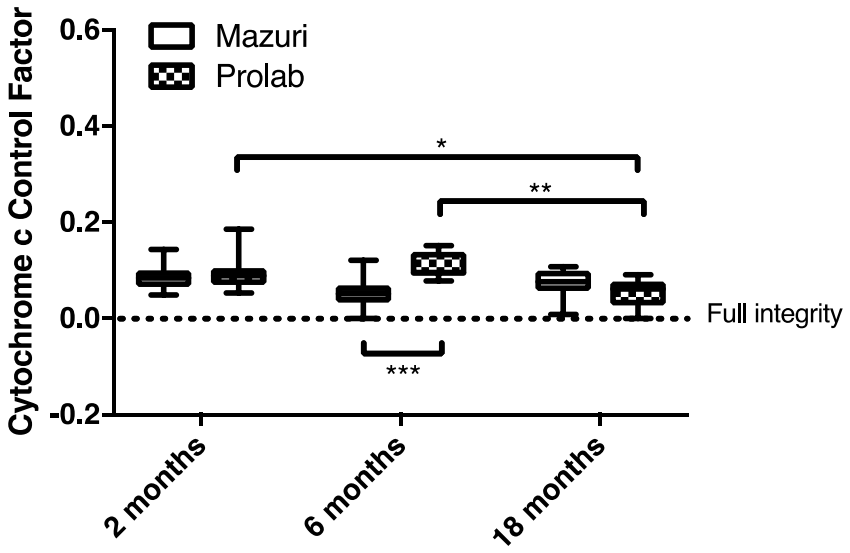

Figure 4.5. Mitochondrial outer membrane integrity expressed as the cytochrome c control factor, which represents the increase in NADH-OXPHOS capacity due to the addition of exogenous cytochrome c. A value of 0.0 indicates full integrity. Two dietary groups (Mazuri and Prolab diets) and three age groups (2 months, 6 months, and 18 months) are included. Data are presented as box plots showing minimum, 25th percentile, median, 75th percentile, and maximum. Significant differences are indicated above the boxes for age differences within a diet, and below the boxes for diet differences within an age group. * $P<0.05$, ** $P<0.01$, *** $P<0.001$. n = 7-12.

A.4.3.2 Mitochondrial OXPHOS capacity; NADH and succinate pathways, and CIV single step

The respiratory capacity expressed as flux per mass (Figure 4.6, A-D) decreased significantly with age, but only in Prolab-fed animals. NADH pathway OXPHOS capacity was significantly decreased in Prolab-fed animals at 18 months compared to 2 month (Tukey test, $p = 0.032$) and 6 month (Tukey test, $p = 0.035$) Prolab-fed animals from the same dietary group (Figure 4.6A). Similarly, Succinate pathway OXPHOS capacity was significantly decreased in Prolab-fed animals at 18 months, compared to the same dietary group at 6 months of age ($p=0.025$; Figure 4.6C). The combined NADH & Succinate pathway followed the same trend without reaching significance ($p = 0.077$, Figure 4.6B). Complex IV activity did not vary significantly with age (Figure 4.6D). The mass specific OXPHOS capacity while feeding electrons into different parts of the ETS did not show significant differences between diets, but an upward trend in NADH & Succinate pathways OXPHOS capacity in 6 month Prolab animals was noted when compared to age-matched Mazuri controls (Tukey test, $p = 0.055$) (Figure 4.6B).

The OXPHOS capacity was then expressed as FCRs, normalized for maximal OXPHOS capacity in the presence of substrates feeding electrons into NADH & Succinate pathways simultaneously. FCRs represent the proportional contribution of various pathways and steps to maximal OXPHOS capacity, and therefore are dictated by mitochondrial properties rather than mitochondrial content. The FCRs for NADH (Figure 4.6E) or Succinate pathway (Figure 4.6G) did not show any difference between age or dietary groups. In contrast, both age and diet significantly affected the FCRs for Complex IV (Figure 4.6H). Interestingly, in contrast to other age-related differences in OXPHOS capacity (shown above, expressed in flux per mass), an aging effect was seen in Mazuri-fed animals rather than Prolab-fed animals. The FCR for Complex IV was significantly increased from 2

months to 6 months in Mazuri fed animals ($p = 0.038$) (Figure 4.6H.), and then decreased at 18 months of age in the same dietary group ($p=0.003$). In addition, FCRs for Complex IV showed an early dietary effect in 2 month animals; CIV FCRs were significantly increased in Prolab-fed animals when compared to age-matched Mazuri-fed controls ($p = 0.037$). These results suggest that early changes in mitochondrial respiratory function are detectable prior to the onset of hyperglycemia in the NR.

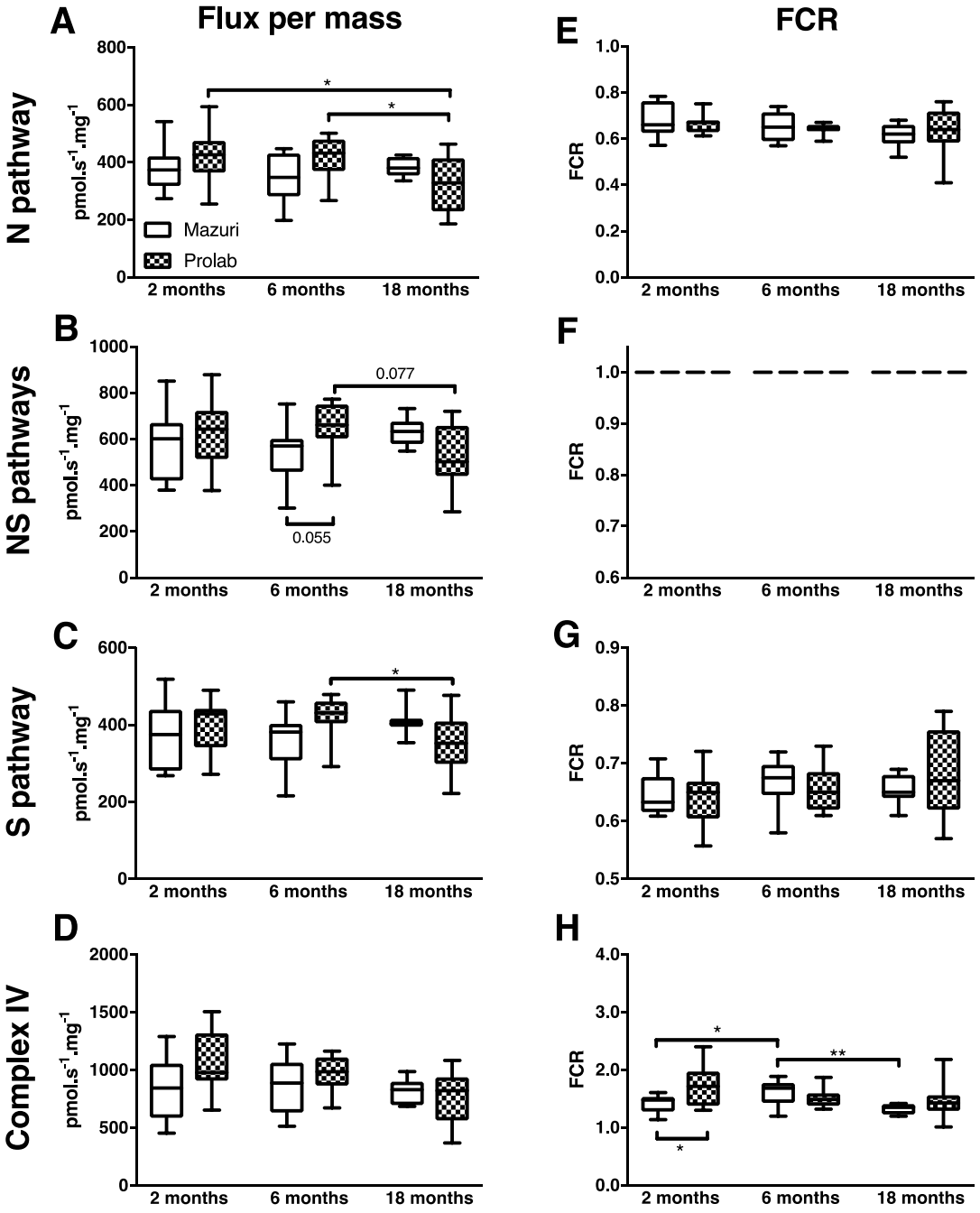

Figure 4.6: Oxidative phosphorylation (OXPHOS) capacity in cardiac permeabilized fibers from Nile rats of two dietary groups (Mazuri and Prolab diets) and three age groups (2 months, 6 months, and 18 months). OXPHOS capacity was expressed in flux per fiber mass (pmol s^{-1} mg^{-1} wet weight, A, B, C, D) or as Flux Control Ratios (FCR; E, F, G, H). The OXPHOS rate was determined in the presence of saturating ADP, cytochrome *c*, and substrate feeding electrons into the NADH pathway (N pathway, pyruvate+malate, A, D), the NADH&Succinate pathways (NS pathways, pyruvate+malate+succinate, B, E), the Succinate pathway (S pathways, Succinate+rotenone, C, G), and the Complex IV single step (D, H). Data are presented as box plots showing minimum, 25th percentile, median, 75th percentile, and maximum. Significant differences are indicated above the boxes for age differences within a diet, and below the boxes for diet differences within an age group. * P<0.05, ** P<0.01. n = 7-12.

A4.3.3 Mitochondrial OXPHOS capacity; Fatty Acid Beta Oxidation

In Prolab-fed NRs, the OXPHOS capacity in the presence of fatty acid substrates did not vary significantly with age (Figure 4.7). In contrast, in Mazuri-fed NRs, the OXPHOS capacity in the presence of octanoylcarnitine+malate was significantly decreased with age (Fig. 4.7B); there is a decrease in OXPHOS capacity at 6 months ($p < 0.001$) and 18 months ($p < 0.044$) when compared to diet-match 2 month animals. The same trend of a decrease in oxidation with age is also observed with other substrates (acetylcarnitine and palmitoylcarnitine) in the Nile rats fed the Mazuri diet, but not in the Prolab fed rats (Figure 4.7A,C).

There was also a dietary effect observed in the NRs at 6 months of age; Prolab-fed animals showed increased fatty acid beta-oxidation with octanoylcarnitine+malate at 6 months when compared to age-matched Mazuri-fed controls ($p = 0.010$) (Figure 7B). The same trend was observed with acetylcarnitine+malate as substrates, but without reaching significance (Figure 4.7A). Interestingly, at 18 months of age, the diet had no effect on fatty acid oxidation capacity with any of the substrates (Figure 4.7 A-C).

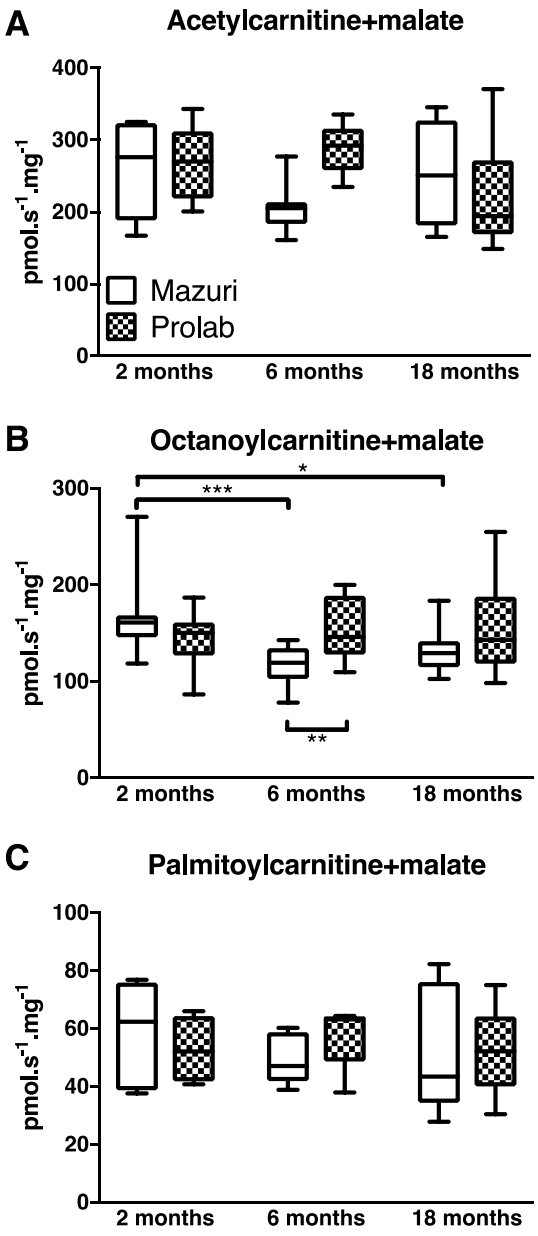

Figure 4.7. Oxidative phosphorylation (OXPHOS) capacity in the presence of fatty acid substrates in cardiac permeabilized fibers from Nile rats of two dietary groups (Mazuri and Prolab diets) and three age groups (2 months, 6 months, and 18 months). OXPHOS capacity was expressed in flux per fiber mass (pmol s^{-1} mg^{-1} wet). The OXPHOS rate was determined in the presence of saturating ADP, cytochrome *c*. The fatty acid substrates combinations included acetylcarnitine+malate (A, n=5-6), octanoylcarnitine+malate (B; n=9-12), and palmitoylcarnitine+malate (C, n=4-10). Data are presented as box plots showing minimum, 25th percentile, median, 75th percentile, and maximum. Significant differences are indicated above the boxes for age differences within a diet, and below the boxes for diet differences within an age group. * $p<0.05$, ** $p<0.01$, *** $p<0.001$, n = 7-12.

A.4.4 Citrate Synthase Activity

Citrate synthase activity was evaluated as a surrogate marker of cardiac ventricular mitochondrial content. Citrate synthase activity was significantly decreased with age in Prolab-fed animals (Figure 4.8), with 2 month animals showing significantly higher activity compared to both 6 ($p = 0.019$) and 18 month-old animals ($p < 0.001$). Furthermore, Prolab-fed animals had increased citrate synthase activity at 2 months compared to age-matched Mazuri-fed animals ($p = 0.002$).

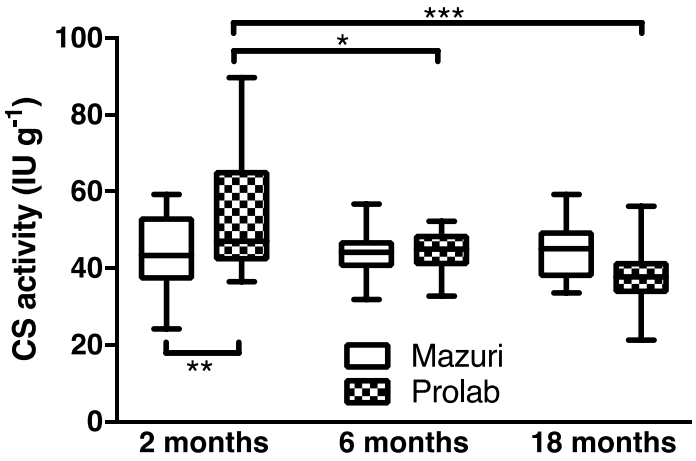

Figure 4.8. ***Dietary and aging effect on mitochondrial citrate synthase activity.*** Samples were tested in triplicate. Data are presented as box and whisker plots of mean CS activity ($IU.g^{-1}$). Data were analyzed using two-way ANOVA, with square root transformation to meet ANOVA assumptions. *$p<0.05$, **$p<0.01$, ***$p<0.001$, $n = 4$-9. CS activity is used as a surrogate marker of mitochondrial content. CS activity was significantly increased at 2 months in Prolab-fed animals compared to age-matched controls.

A.5 Chapter 5 – DISCUSSION

A.5.1 Animal Model

Currently, there are approximately 41 studies utilizing the NR as an experimental animal model. These studies focus on retinal and ophthalmic changes, circadian rhythm/diurnal activity, and neurological structural/functional differences in these animals. There are currently no studies investigating cardiovascular changes in NRs, nor investigating mitochondrial functional changes of any kind in NR cardiac tissue. Our study provides novel contributions to the study of *A. niloticus*, and may introduce the NR as a potential experimental model of T2DM. Furthermore, over the course of this study and other by our lab, signs of disease beyond the scope of the present study were noted during surgical procedures[107]. Fatty livers, hepatic tumours, and cataracts occurred more frequently in older hyperglycemic animals (Figure 5.1). The NR has been studied by our lab as an animal model for retinal circuitry changes associated with diabetic retinopathy[110]. Splenomegaly was discovered incidentally in one Prolab-fed animal at 18 months, which is a rare, but serious complication of T2DM in humans[4]. The enlarged spleen measured 4.7 cm in length, whereas a normal NR spleen measures between 1-1.5 cm in length. Based on these findings, the NR presents a unique opportunity to study the effects of prolonged hyperglycemia and insulin resistance on various organ systems.

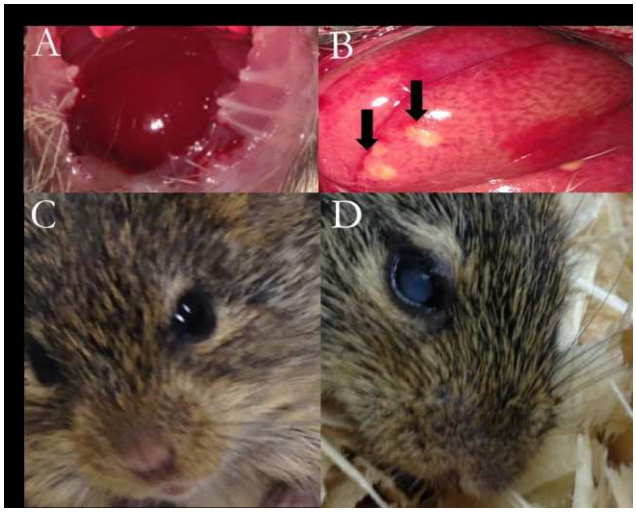

Figure 5.1. Examples of organ systems affected by T2DM in the NR. (A) Appearance of healthy liver in 2 month male Mazuri-fed NR. (B) Evidence of fatty liver deposits and possible hepatic tumours in Prolab-fed male at 18 months. Arrows indicate tumours. (C) Prolab-fed NR showing no visual indications of cataracts at 6 months of age (D) Prolab-fed NR with cataracts at 18 months of age.

A.5.2 Metabolic Profile

Consistent with previous findings by our lab[107] and others[101,106], hyperglycemia became evident at 6 months of age in 67% of male Prolab-fed NRs studied. FBG readings remained within normal limits (<5.0 mmol/L fasting) at 2 months of age in all Prolab and Mazuri-fed animals. FBG readings of Mazuri-fed animals did not suggest hyperglycemia at any age, establishing the Mazuri diet as a control for hyperglycemia. FBG readings were taken immediately prior to euthanasia, to ensure injection of pentobarbital sodium did not distort FBG readings[128]. Manual blood glucose monitoring is a simple and reliable method to measure glucose levels, and it is the most common method used by diabetes patients to manage their glycemic status.

Interestingly, although the average FBG increased in Prolab-fed NRs from 6 months (10.3±3.78) to 18 months of age (11.3±2.82), FBG readings remained in normal range in two 18 month-old Prolabs. Based on the FBG results from previous studies by our lab, Prolab-fed NRs demonstrate fasting hyperglycemia at 12 months of age, suggesting that a metabolic collapse occurs in FBG between 12 and 18 months in some animals. This difference could be explained by increased incidence of abdominal or hepatic tumours noted macroscopically in older animals, as reduced blood glucose may be considered an atypical early sign of hepatocarcinoma[101,129]. Indeed, tumours consume glucose, which could reduce an elevated FBG[130]. Alternatively, insulinomas may reduce FBG secondary to excess secretion of insulin-like growth factor 2 (ILGF-2), however these are rare[130].

In general, plasma insulin levels trended higher in Prolab-fed animals compared to Mazuri-fed controls. Trends in our dataset are suggestive of insulin resistance in the Prolab-fed NRs. This metabolic profile was consistent with other studies done on NRs by our lab and others[101,107]. Our results show an early perturbation in the metabolic profile of the NR,

suggesting insulin resistance is evident as early as 2 months of age. Plasma insulin levels were relatively stable at all endpoints in Mazuri-fed animals. Historical evidence has shown that insulin resistance occurs naturally with age, even in healthy individuals[131,132].

Finally, glycated HbA1c was measured to provide a longitudinal measure of glycemic status. Based on previous work by our lab, and in comparison to Mazuri-fed animals, an HbA1c > 6% was considered elevated in the NR. In concordance with our FBG findings, %HbA1c was significantly increased in Prolab-fed animals at 6 months, compared to age-matched controls. Glycated HbA1c was also elevated at 2 months and 18 months in Prolab-fed animals compared to age-matched controls, but these did not reach significance. The lack of statistical significance at 2 months and 18 months could be attributed to larger variability in FBG readings at these timepoints, suggesting that the metabolic profiles of NRs were in a state of flux. Furthermore, changes in %HbA1c are less obvious in younger animals, as shown by Noda *et al*[101]. Based on the results of the Diabetes Control and Complications trial, Diabetes Canada guidelines recommend a goal %HbA1c of less than 7% for diabetic patients, to reduce the risk of diabetic complications[4].

A.5.3 Transthoracic Echocardiography

Transthoracic echocardiography studies were performed on a subset of 12 month NRs. Echo studies had never been attempted in these animals, and there were limitations (See Section A5.7). Prolab-fed animals were noted to display baseline heart rates (HR) that were elevated compared to Mazuri-fed controls; however, when normalized for body weight, there was no significance ($p = 0.730$). Increasing BMI and/or hip-to-weight ratio is a well-known risk factor for hypertension and other cardiometabolic diseases which may affect heart rate[133]. Cardiovascular autonomic neuropathy is a known complication of severe T2DM that is associated with tachycardia, postural hypotension, cardiac arrhythmias, and

asymptomatic ischemia in humans[134,135]. Cardiovascular autonomic neuropathy progresses from a reduction in parasympathetic tone to ventricular sympathetic denervation that increases propensity for arrhythmias[136]. NRs do not appear to demonstrate early disruption in cardiac autonomic function; however, this was not studied directly, and further longitudinal analysis of blood pressure, heart rate, and electrocardiographic images would allow for further characterization. Interestingly, Noda *et al.* have reported that male diabetic NRs are consistently more hypertensive, and show evidence of macroscopic vascular lesions suggestive of atherosclerosis, suggesting a multifactorial etiology for the development of cardiovascular disease in the NR[101].

Some Prolab-fed animals demonstrated an elevated E/E' ratio. This lead to a trend showing elevated E/E' ratio when compared to Mazuri-fed controls. Although this difference was not statistically significant ($p = 0.0635$), it is an early indicator of diastolic dysfunction that has never been recorded in these rodents. The E/E' ratio represents the ratio between peak mitral inflow velocity and peak early diastolic movement of mitral annulus, giving an indication of left ventricular filling pressure[137]. An increase in the E/E' ratio is indicative of an increase in LV filling pressure, as blood flow into the ventricle exceeds the relaxation capacity of the mitral annulus, affecting time spent in diastole. E/E' ratio has been used to evaluate cardiac function in patients with heart failure, cardiomyopathy, and arrhythmias, and is integral to new LV diastolic function clinical guidelines[53]. Mitral inflow indexes are complex and subject to misinterpretation, as they are affected not only by the properties of the LV, but also by heart rate, left-atrial to LV pressure gradients, and LV compliance.[138] In humans, the utility of the E/E' ratio is affected by the presence of mitral valve disease, moderate to severe mitral annular calcification, left bundle branch block, and constrictive pericarditis, among others[53,139]. This trend in our results

suggests that Prolab-fed NRs are more prone to early indices of LV diastolic dysfunction at 12 months. An additional index of diastolic dysfunction that would support this finding is the left atrial (LA) volume. We would anticipate that the LA volume would be larger in Prolab-fed animals, in compensation for the poor relaxation occurring the LV. However, we were unable to obtain accurate LA measurements in our current study.

Finally, the E'-wave velocity trended lower than the A'-wave velocity in the majority (80%) of Prolab-fed animals on tissue-Doppler imaging (TDI), which is considered an indicator of early diastolic dysfunction. This observation manifested as a reduction in the E'/A' ratios of Prolab-fed animals compared to Mazuri-fed controls, which reached significance. Although this value is not clinically relevant, a difference in E'/A' ratios between groups supports a mild decrease in the E'-wave velocity, combined with a mild increase in the A' velocity. These would not be so large as to show significant changes in the E' wave or the A' wave alone. TDI relies on detecting a shift in frequency by ultrasound waves reflected from moving myocardium. Although limited to detecting only the vector of motion parallel to the ultrasound beam, TDI is an emerging method to assess LV systolic and diastolic function, in humans and animal models of disease.[140] The E'-wave velocity represents the peak early diastolic movement of mitral annulus, and the A'-wave velocity represents the peak late diastolic movement of mitral annulus. A slowing of the E'-wave represents impaired LV relaxation, which is an indicator of diastolic dysfunction.

A.5.4 Cardiac Mitochondrial Function

A.5.4.1 Citrate Synthase Activity

Citrate synthase is a mitochondrial matrix enzyme that catalyzes the condensation of acetyl-CoA with oxaloacetate to generate citrate, which is the first reaction in the citric acid

(TCA) cycle[124]. Our results indicate that citrate synthase activity is significantly higher in 2 month Prolab-fed animals compared to age-matched controls (Figure 8). The increase in mitochondrial content occurred prior to detection of hyperglycemia, but not prior to detection of hyperinsulinemia.

The effect of insulin resistance on mitochondrial content and function has been studied in insulin-sensitive tissues such as skeletal muscle[141], adipose tissue[142], hepatic tissue[143], and cardiac tissue[144]. In general, mitochondrial biogenesis is increased during early stages of insulin resistance, to accommodate a metabolic shift to fatty acid oxidation as the primary mitochondrial fuel. Boudina *et al.* report increased mitochondrial biogenesis in 9 week old *ob/ob* hearts, as shown by an increased ratio of mitochondrial DNA copy number to nuclear DNA copy number[145]. However, despite this apparent increase in mitochondrial content, they still reported reduced expression of ETS complexes under diabetic conditions[146]. This suggests mitochondria may become defective at an early stage of diabetes, despite an increase in mitochondrial content. Electron micrographs of insulin-resistant (but non-hyperglycemic) hearts of 3 month old transgenic mice indicate that mitochondria are larger and greater in number[147]. Larger mitochondria indicate mitochondrial swelling, which is associated with mitochondrial membrane depolarization, and dissipation of the proton gradient[148]. These pieces of evidence support that although mitochondrial content in 2 month NRs is increased, these mitochondria may function poorly. In contrast, recent evidence by Morrow *et al.* suggests that increased mitochondrial content could offer beneficial resistance to metabolic effects of T2DM, using a mouse model deficient in adenine nucleotide translator isoform 1 (ANT1)[149]. ANT1 is an inner mitochondrial membrane translocator localized to the heart, muscle, and brain, whose primary role is to exchange mitochondrial ATP for cytosolic ADP. Mice with a deletion of

ANT1 present with myopathy and hyperproliferation of skeletal muscle mitochondria. The authors demonstrated that hyperproliferation of skeletal muscle mitochondria improved insulin sensitivity, restored glucose tolerance, and reduced susceptibility to toxic effects of high fat feeding, despite increasing evidence of mitochondrial ROS and uncoupling[149]. Therefore, increasing mitochondrial content may prove adaptive under conditions of T2DM.

The early biogenic response by mitochondria ultimately fails as insulin resistance progresses to outright hyperglycemia. Citrate synthase activity was increasingly reduced with advancing age and disease in Prolab-fed animals. Although there is evidence concerning cardiac mitochondrial content in early T2DM, evidence at later stages of disease progression is poor. It has been shown that mitochondrial content in skeletal muscle decreases as the severity of T2DM increases[150]. As NRs did not show hyperglycemia until 6 months of age, our results suggest that hyperglycemia may enhance aging-related changes to mitochondrial content. This is supported by the fact that there were no significant differences in mitochondrial content in Mazuri-fed animals. Mitochondrial exposure to hyperglycemic conditions induces fragmentation, as shown in cell culture in various tissue types, including the heart[91]. The precise mechanism of mitochondrial fragmentation under hyperglycemic conditions is unknown; however, it is directly mediated by dynamin-related protein 1 (DRP-1) in mammals[151]. Mitochondrial fragmentation is associated with increased ROS and subsequent ROS-induced release of apoptotic mediators, including caspases[91] This may occur due to rearrangement of ETS complexes during fragmentation, which could compromise its integrity, and prime downstream pro-apoptotic pathways. Although it has been proposed that mitochondrial fragmentation may be induced in preparation for mitochondrial apoptosis, conflicting evidence has shown that exodus of mitochondrial apoptotic factors such as adenylate kinase 2 still occurs when mitochondrial fission is

inhibited[152]. Therefore, the link between mitochondrial fragmentation, fission, and apoptosis remains unclear.

A.5.4.2 Mitochondrial coupling

LEAK respiration is a functional representation of the extent of mitochondrial coupling. As the inner mitochondrial membrane is inherently permeable to protons, unregulated proton leak occurs under physiological conditions, which means that mitochondrial oxygen consumption and ATP synthesis are incompletely coupled *in vivo*[153]. This non-ohmic basal leak is required for mitochondrial function in the absence of ADP, as mitochondria continue to consume oxygen under non-phosphorylating conditions[154]. Other inducible pathways of proton leak, such as uncoupling proteins (UCPs), and the adenosine monophosphate/adenine nucleotide translocase (AMP/ANT) system are in place to provide more robust avenues of proton leak [155]. In both cases, however, redox energy is dissipated as heat, rather than being used to power ATP synthesis. In our study, LEAK respiration measured in the presence of substrates feeding electrons into the NADH pathway (PM) was used as an indicator of coupling

Our results did not indicate a difference in LEAK respiration expressed in flux per mg between diets. However, when LEAK was expressed as a FCR, a significant drop was detected at 6 months in Prolab-fed animals compared to controls (Figure 4.4). This result was reversed at 18 months, where the FCR for LEAK in Prolab-fed animals was significantly increased compared to controls. These differences in FCR are independent of mitochondrial content, and suggest tighter coupling at 6 months in Prolab-fed animals, followed by poorer coupling by 18 months in the same dietary group. Tighter coupling involves a maintenance of the mitochondrial membrane potential, and a more efficient use of the proton-motive

force to generate ATP, whereas looser coupling involves dissipation of proton-motive force for ATP synthesis.

Results from Boudina *et al.* have shown that uncoupling of cardiac mitochondria occurs in both *ob/ob*[146] and *db/db*[156] animal models. The authors propose increased delivery of fatty acid substrates to the heart increases the production of ROS and lipid peroxidation products, activating proton leak through UCP3 and adenine nucleotide translocase (ANT) pathways[145]. UCP3 is primarily expressed in the heart, and is mediated by free fatty acids, lipid peroxidation products and ROS[157]. UCP3 is thought to perpetuate high rates of FAO by exporting fatty acid anion (FA^-) from the mitochondrion, after mitochondrial thioesterase hydrolyzes fatty acyl-CoA to regenerate free CoA[88,158]. ANT is a translocase also localized to the inner mitochondrial membrane, that is involved in the back transport of deprotonated long-chain fatty acids. ANT1 is the primary isoform expressed in the human heart, and it has been studied for its role in fatty acid-mediated uncoupling[145,159]. The discrepancy between our results and the results of Boudina *et al.* could be explained by the age of animals at the time of study. Evidence of mitochondrial uncoupling by Boudina *et al.* was reported between 8 and 9 weeks of age in *ob/ob* and *db/db* hearts. Prolab-fed NRs did not show evidence of increased uncoupling at a similar age (2 months), but showed tighter coupling at 6 months, and then lesser coupling at 18 months. This suggests that tighter coupling at 6 months by the NR may be a compensatory response, followed by a decompensation response at 18 months. The rapid onset of mitochondrial uncoupling in *ob/ob* and *db/db* rodents may be inherent to the animal model, because they both involve genetic defects in leptin signalling, whereas T2DM is induced in the NR through dietary means[160]. Recent findings have shown tighter mitochondrial coupling occurs in hepatic mitochondria of 6-month-old type I and type 2 diabetic mice[161]. Similar to the NR at 6 months, these animals were hyperglycemic

when changes in mitochondrial coupling were recorded. The authors discussed the decrease in proton conductance and increase in mitochondrial membrane potential as an adaptation to preceding oxidative stress. This suggests that tighter coupling at 6 months in the NR may be to compensate for preceding oxidative stress, induced by hyperglycemia and hyperinsulinemia. This also supports that the increase in LEAK FCR (increased uncoupling) at 18 months represents a decompensation response, because hyperglycemia and hyperinsulinemia persisted in 18 month Prolab-fed animals. Although small amounts of mitochondrial uncoupling are considered protective, significant uncoupling may collapse the mitochondrial membrane potential, producing oxidative stress and disrupton[162]. Yet, it is challenging to establish a threshold for small versus large increases in LEAK respiration, and determine to what extent a change in LEAK respiration is beneficial.

A significant decrease in the LEAK respiration expressed in flux per mg and FCR occurred in Prolab-fed animals between 2 months to 6 months, followed by a significant increase in the LEAK respiration FCR from 6 months to 18 months in the same group. There were no significant changes in LEAK respiration between age groups in Mazuri-fed animals. This suggests that the Prolab diet induced the onset of aging-related changes in mitochondrial coupling (more coupled at 6 months, less coupled at 18 months), whereas Mazuri-fed animals were protected.

Evidence by Serviddio *et al.* on aging rat hearts shows that aged mitochondria experience proton leaks at lower membrane potentials, which suggests that their inner membranes are more permeable to protons[163]. They also show that mitochondrial membrane potentials are decreased with aging, which may impair ATP synthesis up to 8% per decade[164]. These findings suggest that mitochondria are more prone to uncoupling with increasing age. However, Mazuri-fed animals did not demonstrate significant changes in LEAK respiration

with aging. The mitochondrial theory of aging suggests that mitochondrial DNA (mtDNA) mutations accumulate with advancing age, leading to ETS dysfunction, inducing mitochondrial uncoupling and perpetuating a vicious cycle of ROS and further DNA damage[165]. Yet, more recent evidence suggests that mtDNA mutations may not accumulate with age, and a low level of mitochondrial uncoupling and ROS may confer a longevity advantage[164,166]. Thus, there may be fewer aging-related changes in mitochondrial uncoupling than previously thought.

As demonstrated by the aging-related increase in LEAK FCR between Prolab-fed animals at 6 months and 18 months, the presence of T2DM affected aging-related changes in mitochondrial uncoupling. Evidence from several sources implicates mitochondrial ROS and oxidative stress as a source of damage in aging mitochondria. Superoxide damages mitochondria through several mechanisms, such as mitochondrial DNA damage, degradation of respiratory protein complexes, and changes in membrane permeability. Although superoxide levels increase naturally with aging, oxidative damage could be exacerbated by chronic exposure to hyperglycemia or hyperinsulinemia[167]. For example, adult rat cardiomyocytes exposed to hyperglycemia release higher levels of superoxide anion into the experimental media[167,168]. Conversely, work by Hoehn *et al.* in cellular models of insulin resistance has demonstrated that excess superoxide from CIII of the ETS is sufficient to impede translocation of GLUT4 translocators in myotubes, perpetuating insulin resistance[169]. This suggests that oxidative stress is both a potential cause and consequence of insulin resistance, creating a vicious cycle. In addition, damage-prone aged mitochondria may experience attenuation of structural integrity over time, which could contribute to the degree of uncoupling. Therefore, oxidative stress induced by T2DM may play a critical role in inducing aging-related mitochondrial uncoupling in Prolab-fed NRs at 18 months.

A.5.4.3 Mitochondrial Membrane Integrity

The quality of preparations using a combination of manual and chemical methods to permeabilized cardiac fibres was confirmed by results showing minimal control of respiration by exogenous addition of cytochrome *c*. Hyperglycaemic Prolab-fed animals at 6 months showed poorer outer membrane integrity than Mazuri-fed controls. One major difference between Prolab-and Mazuri NRs at 6 months is the presence of hyperglycemia. Microscopy studies of aortic smooth muscle cell mitochondria have shown that the integrity of the outer and inner membrane mitochondrial is increasingly degraded with prolonged exposure to hyperglycemia, with investigators reporting outer membrane losses in 60% of mitochondria after 5 months[170]. This suggests a significant role for hyperglycemia in increasing membrane fragility.

Changes in membrane intactness were also noted with advancing age, with an age-related decline in integrity in Prolab-fed animals at 6 months, followed by an increase at 18 months. A certain degree of loss in integrity occurs naturally in the outer mitochondrial membrane with aging, but our results show the opposite, as membrane integrity was increased in Prolab-fed animals at 18 months. Here, it is likely that hyperglycemia and insulin resistance enhanced the aging effect at an earlier age (manifesting at 6 months)[170]. Evidence using cardiac mitochondria from insulin-resistant aging dogs has shown that mitochondrial integrity is reduced with aging, compared to activity-matched younger controls[171]. The increase in intactness at 18 months is not due to increased mitochondrial content, as we observed decreased citrate synthase activity at 18 months in Prolab-fed animals, which suggests a decrease in mitochondrial content. In addition, it is likely not due to loss of hyperglycemic conditions, as only a small percentage of Prolab-fed animals showed normoglycemia at 18 months. However, because we noted a decline in mitochondrial

content, this could suggest a hyperglycemia-induced loss of active mitochondria. This would leave behind mitochondria whose membranes are more robust, and functionally adapted to hyperglycemic conditions. Support for this idea would require additional studies on mitochondrial structural integrity in cardiomyocytes in the NR.

A.5.4.4 NADH and succinate pathways: OXPHOS Capacities

Mitochondrial OXPHOS capacity of the NADH and Succinate pathways was largely undisturbed by dietary defects at all three time points. The only trend for apparent diet-induced change occurred in the NADH & Succinate pathways expressed in flux per mg, with 6 month animals demonstrating higher OXPHOS capacity than controls. This trend indicated higher convergent electron flux through these pathways, and a higher maximal OXPHOS capacity. Because no change in citrate synthase activity was detected in 6 month Prolab-fed animals, the results suggest a change in mitochondrial properties is responsible rather than mitochondrial content. A possible explanation for the trend in OXPHOS capacity with convergent flow through the NADH & Succinate pathways is the tighter mitochondrial coupling seen at 6 months in Prolab-fed animals. Tighter coupling suggests that the oxidative and phosphorylation systems are functioning more efficiently, which could permit a higher OXPHOS capacity by existing mitochondria. Control of electron transfer through the NADH and Succinate-linked pathway rests largely upstream with the dehydrogenases of the TCA cycle, and is associated with a corresponding excess capacity for downstream respiratory complexes[114,172]. Measurement of NADH-pathway OXPHOS with administration of PM involves a measurement of PDC activity, which did not show significant defects in Prolab-fed NRs at any age. This disagrees with historical evidence suggesting that insulin resistance and DM is strongly correlated with decreased activity of the PDC[173]. Other studies also report a decline in CI (NADH pathway)[80] and CII (Succinate

pathway)[82] respiratory flux, which conflicts with our results. Interestingly, no change in OXPHOS with administration of PM was observed in the heart of fructose-fed rats, despite a decline in PDC activity[67]. Although PDC activity was not directly measured, this indicates that the control of OXPHOS capacity may not be determined by upstream dehydrogenases under diabetic conditions in the NR.

The increase in mitochondrial content seen in 2 month Prolab animals did not occur with a concurrent increase in maximal OXPHOS capacity through the NADH & Succinate pathways. This is maladaptive, because increasing mitochondrial content without a simultaneous increase in OXPHOS capacity promotes the accumulation of mitochondrial ROS, without improving the rate of ATP production[174]. A possible explanation for this disconnect between mitochondrial content and capacity is an increase in LEAK capacity (expressed in flux per mg) seen in Prolab-fed animals at 2 months; however, this result did not reach significance. Increased capacity for LEAK respiration would reduce the efficiency of electron flux through the ETS, largely mitigating mitochondrial capacity for increased maximal OXPHOS.

Our results demonstrate that aging defects in OXPHOS capacity in the NADH and Succinate pathways were prevented by the Mazuri diet. This is a major finding of this study, as NRs were fed *ad libitum*, and there are few diets that have been shown to affect age-related defects in mitochondrial function. Defects were observed primarily in the OXPHOS capacity of the NADH pathway in Prolab-fed animals (expressed as flux per mass), with a significant decline in OXPHOS capacity from 2 months and 6 months to 18 months. This suggests that components of the NADH pathway in cardiac mitochondria may be particularly susceptible to aging-related defects in T2DM. An additional decline in OXPHOS capacity expressed in flux per mass was noted in the Succinate pathway, from 6 months to

18 months. Finally, a trend suggested an aging-related decline in NADH & Succinate pathway OXPHOS capacity between 6 month and 18 month Prolab-fed animals. This trend suggests a reduction of maximal OXPHOS, which may be explained by the concurrent decline in the OXPHOS capacities of the NADH and Succinate pathways in isolation. It could also be attributed to the age-related loss of mitochondrial content seen in Prolab-fed animals at 18 months. No aging-related defects occurred in these pathways in Mazuri-fed animals.

These key findings of our study underscore the impact dietary habits can have on aging-related changes in mitochondrial function. In the wild, NRs consume vegetative grasses, seeds, and insects, based on their seasonal availability, and distance from the colony[102]. Thus, their natural diet is rich in fibre and protein, and contains lower amounts of fat. The Prolab diet contains 9.6% fat and 3.2% fibre, and is considered standard chow for laboratory rats. Comparatively, the Mazuri-fed diet contains significantly lesser fat (4.1%) and higher fibre (15%). Protein content is essentially equal between the two diets (Prolab 19%, Mazuri 20%). Prolab-fed NRs are consuming a high fat diet relative to their natural diet, and this may enhance aging-related changes in cardiac mitochondrial OXPHOS capacity through the NADH and Succinate pathways. Both short-term and life-long caloric restriction have proven beneficial, such as reducing evidence of left ventricular hypertrophy and diastolic dysfunction, reducing formation of mitochondrial H_2O_2, and rescuing aging-related defects in mitochondrial function, such as declining OXPHOS capacity; thus, caloric excess is a contributing factor to the onset of aging-related mitochondrial defects[175,176].

Historical bioenergetic studies using isolated mitochondria from rat heart and liver have shown progressive decline in electron transport activities of mitochondrial protein complexes with advancing age[177]. More recent findings using human muscle biopsies have

also shown a decline in mitochondrial respiratory activity, associated with a reduction in ATP production[178]. According to a review by Lee and Wei, an aging-related decline in mitochondrial OXPHOS capacity occurs in parallel with changes in mitochondrial morphology, accumulating mitochondrial DNA mutations, and increasing ROS and oxidative damage[179]. Following the free-radical theory of biology, as CI is a significant contributor to ROS production, a significant reduction in NADH-pathway OXPHOS capacity may protect NR cardiac mitochondria from accumulating ROS[180]. However, more recent evidence suggests that aging-related mitochondrial dysfunction may originate from a different upstream pathway, in response to reduced activity of histone deacetylase SIRT1[181]. By activating SIRT1 activity with NAD^+, Gomes *et al.* showed significant reversal of an aging-related decline in mitochondrial respiratory function[181]. SIRT1 regulates mitochondrial function through deacetylation of PGC-1α, a nuclear transcription factor implicated in mitochondrial biogenesis. In extension to these findings, Shadel *et al.* suggest a cascade of events occurring in the nucleus -including a decline in SIRT1 activity - leading to a decline in mitochondrial gene expression and poor OXPHOS performance[182]. SIRT1 has been widely discussed as a therapeutic target for T2DM[183]. Further study is required to determine the role of SIRT1 signalling in age-related changes in OXPHOS capacity in T2DM.

A.5.4.5 CIV Single Step Activity

Mitochondrial CIV catalyzes electron transfer from reduced cytochrome *c* to terminal oxygen, producing water at the final stage of the ETS. Whereas there were no significant changes in CIV activity in flux per mg of fibers, our results showed significant changes when expressed as FCR. A significant increase in the FCR for CIV was observed in 2-month Prolab-fed animals, when compared to Mazuri-fed age-matched controls. This suggests that

there was higher capacity, and lesser control by CIV early in the pathogenesis of T2DM in the NR. As there was no change in maximal OXPHOS, the increased capacity of CIV for electron flux occurred irrespective of mitochondrial content. The proportion and activity of CIV varies according to environmental conditions and some experimental evidence suggests this may occur to reduce the release of oxygen free radicals[184]. Under increasingly pro-oxidant conditions, the catalytic efficiency of CIV has been shown to improve[184]. On the other end, reduced CIV capacity is associated with energy crisis (reduced ATP production), lactic acidosis, and increased formation of mitochondrial ROS[185]. Targeted studies using stable expression of shRNA to target CIV subunit mRNA have shown that limiting CIV capacity to 10% of normal is associated with a massive release of ROS. It is well accepted that T2DM is associated with increased cellular levels of ROS and oxidative stress[43,151]. Our results showing an increase in FCR for CIV at 2 months in Prolab-fed animals suggest an early compensatory mechanism to prevent ROS production. On the other hand, recent findings by Friday *et al.* suggest that CIV OXPHOS capacity is reduced after as little as 1 month of exposure to hyperglycemia and insulin deficiency, but no measurements were performed at an earlier stage in that study, to show what occurred prior to the onset of hyperglycemia[186]. This suggests that hyperglycemia may induce differential effects on CIV OXPHOS, as NRs were not hyperglycaemic at 2 months.

Contrary to expectations, an aging-related change in FCR for CIV capacity occurred in Mazuri-fed animals, with statistically significant increase occurring between 2 months and 6 months, and a decrease occurring between 6 months and 18 months. In contrast, there were no aging-related changes in FCR for CIV capacity in Prolab-fed animals, but the high FCR in Prolab-fed animals at 2 months indicates that the increase occurred earlier in Prolab-fed animals compared to Mazuri-fed. Historical work by Paradies *et al.* demonstrated that

CIV OXPHOS capacity is reduced in the cardiac mitochondria of healthy aged rats, while the mitochondrial content remained the same[187]. Our findings suggest that the Prolab diet may affect the natural change in CIV capacity associated with aging. Increasing CIV capacity may be protective in terms of ROS production, as discussed above. However, recent findings using knockout mice have shown that limiting CIV assembly promotes longevity, improves insulin sensitivity, and increases expression of peroxisome-proliferator-activated receptor ɣ-coactivator 1-α mRNA and protein, as well as its target genes which promote mitochondrial biogenesis[188]. Based on these recent findings, the CIV response to T2DM in the NR may be an aggravated increase in flux control to compensate for the ongoing disruption upstream in the ETS.

A.5.5 Fatty Acid Beta Oxidation

FAO involves the breakdown of short, medium, long, and very-long chain FAs into two-carbon bodies such as acetyl-CoA, for use in other metabolic pathways such as the TCA cycle. As previously stated, FAO is significant contributor to cardiac oxidative energy metabolism, providing up to 70% of cardiac ATP[85]. T2DM induces a loss of metabolic flexibility by the heart, characterized by increased dependence on FAO as an energy source, with reports of up to 90% provision of cardiac ATP by FAO. This occurs less due to cellular failure of glucose uptake, and more due to increasing circulating FAs, leaving little room for glucose oxidation[85]. Our results suggest that NR hearts have a higher OXPHOS capacity for FAO at 6 months in Prolab-fed animals, at least when using octanoylcarnitine as the substrate. A similar trend was also observed with acetylcarnitine as the substrate, but this did not reach significance. The importance of these findings is underscored by similar findings in the fructose-fed model of early reversible T2DM, which showed a significant increase in

OXPHOS with octanoylcarnitine, and a non-significant trend in acetylcarnitine OXPHOS[67]. These results occurred after 6 weeks of fructose feeding, whereas they were not observed until 6 months of age in Prolab-fed NRs. Separate dietary approaches for the induction of T2DM (100g/L fructose supplemented water versus standard rat chow) in these studies may account for this difference[67]. Our results showing no change in oxidation with palmitoylcarnitine present the possibility that the change in OctCar oxidation is due to variation in carnitine translocase or carnitine palmitoyltransferase II (CPTII), which are necessary for the oxidation of both long and medium-chain fatty acids. Carnitine translocase is responsible for shuttling acylcarnitine and carnitine in the mitochondrion, and CPTII converts imported acylcarnitines back into fatty acyl CoA molecules, which serve as substrates for FAO[85]. Oxidation of octanoylcarnitine also occurs through activation of rate-limiting enzyme medium-chain acyl-CoA dehydrogenase (MCAD). MCAD activity is reportedly increased in skeletal muscles of high-fat-fed Wistar rats, obese Zucker rats, and *db/db* mice[189]. However, it is unclear whether similar changes arise in the diabetic heart of the NR.

In concordance with our results, evidence from other animal models of T2DM induced by short-term high fat feeding indicate that FAO is increased at early stages of disease development[190,191,192]. However, at a more advanced stage of T2DM, rates of FAO tend to decline, as shown in studies of skeletal muscle from rats[193], and humans[41]. Aging-related changes in cardiac mitochondria are selectively localized to interfibrillar mitochondria (IFM), whereas subsarcolemmal mitochondria (SSM) appear more resistant to aging-related changes to oxidative phosphorylation[194]. Our study did not selectively isolate subtypes of cardiac mitochondria. Interestingly, an aging-related decline in OXPHOS capacity for fatty acids was not observed in Prolab-fed animals. The age-related change was only observed in

Mazuri-fed animals, leading to a higher rate of octanoylcarnitine oxidation at 2 months compared to both 6 months and 18 months. The preservation of FAO throughout the age range in Prolab-fed animals may serve a mild protective role, as aging defects in cardiac mitochondria are probable contributors to chronic oxidative injury, such as increased generation of H_2O_2 and oxygen radicals[195]. However, it is more likely that chronic FAO leads to excess circulating reducing equivalents of NADH and $FADH_2$, providing electrons to the NADH-pathway and Q-cycle, respectively[196]. This increases the reduction potential of the ETS and promotes electron leakage to adaptively dissipate the rising mitochondrial membrane potential, leading to the formation of superoxides from CI and favoring reduced ubiquinol over ubiquinone[197]. Excess $FADH_2$ from fatty acid substrates promotes the formation of superoxide at the Q cycle by: 1) reducing the availability of ubiquinone for electron receipt from CI, 2) promoting reverse electron transfer to CI, leading to leakage of electrons, and 3)increasing the driving force for electron flux through CIII[196]. Based on this evidence, chronic maintenance of high FAO rates is likely a maladaptive change occurring in the cardiac mitochondria of Prolab-fed animals, which contributes increased oxidative stress in the heart. Future aconitase activity studies in the NR heart will provide a clearer image of the redox environment of the NR heart.

A.5.6 Significance

Taken together, our salient findings suggest that there is discernable mitochondrial dysfunction occurring early in the pathogenesis of T2DM in the NR heart, prior to the onset of hyperglycemia. It is remarkable that poor dietary habits may manifest as early as 2 months, and illustrate how rapidly metabolic adaptations start to occur. Our results provide novel contributions to the study of *A. niloticus*, and provide preliminary evidence that the NR may serve as a useful experimental model for the study of cardiac derangements in T2DM. We

show preliminary evidence of early indices of diastolic dysfunction occurring in the NR at 12 months of age. Furthermore, our results have provided a deeper understanding of the mitochondrial functional defects occurring during the progression of T2DM in the NR. Given the increasing prevalence of T2DM worldwide, these results emphasize the importance of preventing the onset of early changes, to prevent later disease progression. Therapeutic implications of this study emphasize mitochondrial structures as potential therapeutic targets, as therapies targeting mitochondria may provide novel means to treat or minimize diabetes complications

A.5.7 Limitations

The interpretation of findings of this study may be affected by the following limitations:

1. Our NR colony originated from 29 animals, brought from Africa for the study of circadian rhythm. Although we assume random genetic diversity in our colony, it is necessary to acknowledge the possibility of inbreeding, and the effect it may have on the presentations of the phenotypes we have reported.
2. Our metabolic and respirometry experiments had low n-numbers, which may limit our ability to accurately detect difference between gruops
3. To our knowledge, echocardiographic assessment of NRs has never been attempted prior to this study. Echocardiographic assessment was very challenging, as barrel chest of the NR displaced the heart from the anticipated location.
4. An intermediate sized echocardiography probe would have provided clearer images for analysis; however, this was not available at the time of study.
5. Animals were not fasted prior to echocardiographic assessment, so it is difficult to speculate on their metabolic conditions at the time of echo measurements.

6. Additional echocardiographic studies using additional NRs are necessary to confirm the existence of cardiac functional changes in Prolab-fed animals.
7. Serial measurement of FBG would provide a more comprehensive metabolic picture of the NR progression into T2DM; however, this was not attempted to avoid undue stress onto NRs from frequent handling.
8.

A.5.8 Future Directions

In response to the limitations listed above, the Sauvé laboratory is currently planning to undertake additional experiments in support of these findings in NR cardiac mitochondria. These may include:

1. Echocardiographic assessments of NRs at additional time points, to provide a more comprehensive profile of cardiac function in these animals.
2. Measurements of oxidative stress in cardiac tissues, such as assays for aconitase enzymatic activity, or 4-hydroxynonenal (HNE) staining to provide an indication of the oxidative environment of cardiac mitochondria at each stage of disease progression.
3. Examinations of mitochondrial enzyme content and activity (specific to medium- and long-chain FAO), as an avenue to explain the increase in octanoylcarnitine oxidation seen at 6 months.
4. A series of high resolution respirometry protocols performed using permeabilized cardiac fibres at additional time points (NRs younger than 2 months, and intermediate to 6 and 18 months), to reveal changes in mitochondrial function as they occur in a longitudinal manner.

5. Measuring expression of signalling pathway components, such as sirtuins, could provide clarity on the mechanistic progression of T2DM in the NR.

REFERENCES

1. International Diabetes Federation. *IDF Diabetes Atlas*. (2015).
2. Dudley, P. Diabetes in Canada. *Stride* (2003).
3. Pickup, J. C. & Williams, G. *Textbook of Diabetes. Internal Medicine* **1,** (Wiley-Blackwell, 2003).
4. Clinical Practice Guidelines. *Can. J. Diabetes* **37,** 212 (2013).
5. Yu, H. *et al.* Initiating Characteristics of Early-onset Type 2 Diabetes Mellitus in Chinese Patients. *Chin. Med. J. (Engl).* **129,** 778 (2016).
6. Ronald Goldenberg MD, FRCPC, FACE, Zubin Punthakee MD, MSc, F. CDA Clinical Practice Guidelines - Chapter 3: Definition, Classification and Diagnosis of Diabetes, Prediabetes and Metabolic Syndrome. *Can J Diabetes* 212 (2013). Available at: http://guidelines.diabetes.ca/browse/Chapter3. (Accessed: 14th January 2016)
7. Zhang, X. *et al.* A1C level and Future Risk of Diabetes: A systematic review. *Diabetes Care* **33,** 1665–1673 (2010).
8. Booth, G. *et al.* Pharmacologic Management of Type 2 Diabetes: 2016 Interim Update. *Can. J. Diabetes* **40,** 484–486 (2016).
9. Heaf, J. Metformin in chronic kidney disease: time for a rethink. **34,** 353–357 (2014).
10. Brownlee, M. & Brownlee. Biochemistry and molecular cell biology of diabetic complications. *Nature* **414,** 813–20 (2001).
11. Aydeniz, A., Gursoy, S. & Guney, E. Which musculoskeletal complications are most frequently seen in type 2 diabetes mellitus? *J. Int. Med. Res.* **36,** 505–511 (2008).
12. Huxley, R., Ansary-Moghaddam, A., Berrington de González, A., Barzi, F. & Woodward, M. Type-II diabetes and pancreatic cancer: a meta-analysis of 36 studies. *Br. J. Cancer* **92,** 2076–83 (2005).

13. Hu, F. B. *et al.* Prospective study of adult onset diabetes mellitus (type 2) and risk of colorectal cancer in women. *J. Natl. Cancer Inst.* **91,** 542–547 (1999).

14. Turner, R. C. *et al.* Intensive blood-glucose control with sulphonylureas or insulin compared with conventional treatment and risk of complications in patients with type 2 diabetes. **352,** 837–853 (1998).

15. Patel A, MacMahon S, Chalmers J, Neal B, Billot L, Woodward M, Marre M, Cooper M, Glasziou P, Grobbee D, Hamet P, Harrap S, Heller S, Liu L, Mancia G, Mogensen CE, Pan C, Poulter N, Rodgers A, Williams B, Bompoint S, de Galan BE, Joshi R, T. F. Intensive Blood Glucose Control and Vascular Outcomes in Patients with Type 2 Diabetes. *N. Engl. J. Med.* **358,** 2560–2572 (2008).

16. Mitnick, C. D. *et al.* Effects of Intensive Glucose Lowering in Type 2 Diabates. *N. Engl. J. Med.* **358,** 563–574 (2008).

17. Miccoli, R., Penno, G. & Del Prato, S. Multidrug treatment of type 2 diabetes: A challenge for compliance. *Diabetes Care* **34,** (2011).

18. Grant, R. W., Devita, N. G., Singer, D. E. & Meigs, J. B. Polypharmacy and medication adherence in patients with type 2 diabetes. *Diabetes Care* **26,** 1408–1412 (2003).

19. Cheng, A. Y. Y. Introduction Canadian Diabetes Association Clinical Practice Guidelines Expert Committee. *Can. J. Diabetes* **37,** S1–S3 (2013).

20. Shah, M. S. & Brownlee, M. Molecular and Cellular Mechanisms of Cardiovascular Disorders in Diabetes. *Circ. Res.* **118,** 1808–1829 (2017).

21. Enomoto, M. *et al.* Subendocardial Systolic Dysfunction in Asymptomatic Normotensive Diabetic Patients. *Circ J* **79,** 1749–1755 (2015).

22. Fontes-Carvalho, R., Ladeiras-Lopes, R., Bettencourt, P., Leite-Moreira, A. &

Azevedo, A. Diastolic dysfunction in the diabetic continuum: association with insulin resistance, metabolic syndrome and type 2 diabetes. *Cardiovasc. Diabetol.* **14,** 4 (2015).

23. Dawson, A., Morris, A. D. & Struthers, A. D. The epidemiology of left ventricular hypertrophy in type 2 diabetes mellitus. *Diabetologia* **48,** 1971–1979 (2005).

24. Chait, A. & Bornfeldt, K. E. Diabetes and atherosclerosis: is there a role for hyperglycemia? *J. Lipid Res.* **50 Suppl,** S335–S339 (2009).

25. Saito, S. *et al.* Glucose fluctuations increase the incidence of atrial fibrillation in diabetic rats. *Cardiovasc. Res.* **104,** 5–14 (2014).

26. Richard, J., Ruth, L., Amanda, I. & Irene, M. Risk Factors for Myocardial Infarction Case Fatality and Stroke Case Fatality in Type 2 Diabetes. *Diabetes Care* **27,** 201–207 (2004).

27. Gregg, E. W., Sattar, N. & Ali, M. K. The changing face of diabetes complications. *Lancet* **4,** 537–547 (2016).

28. Gilca, G.-E. *et al.* Diabetic Cardiomyopathy: Current Approach and Potential Diagnostic and Therapeutic Targets. *J. Diabetes Res.* **2017,** 1310265 (2017).

29. Avogaro, A., Vigili De Kreutzenberg, S., Negut, C., Tiengo, A. & Scognamiglio, R. Diabetic cardiomyopathy: A metabolic perspective. *Am. J. Cardiol.* **93,** 13–16 (2004).

30. Boudina, S. & Abel, E. D. Diabetic Cardiomyopathy Revisited. *Circulation* **115,** 3213–3223 (2007).

31. Rubler, S. *et al.* New type of cardiomyopathy associated with diabetic glomerulosclerosis. *Am. J. Cardiol.* **30,** 595–602 (1972).

32. Faria, A. & Persaud, S. J. Cardiac oxidative stress in diabetes: Mechanisms and therapeutic potential. *Pharmacol. Ther.* **172,** 50–62 (2017).

33. Kiencke, S. *et al.* Pre-clinical diabetic cardiomyopathy: Prevalence, screening, and

outcome. *Eur. J. Heart Fail.* **12,** 951–957 (2010).

34. Van Heerebeek, L. *et al.* Diastolic stiffness of the failing diabetic heart: Importance of fibrosis, advanced glycation end products, and myocyte resting tension. *Circulation* **117,** 43–51 (2008).

35. Campbell, F. M. *et al.* A Role for Peroxisome Proliferator-activated Receptor (PPARa) in the Control of Cardiac Malonyl-CoA Levels. *J. Biol. Chem.* **277,** 4098–4103 (2002).

36. Sakamoto, J. U. N. *et al.* Contribution of malonyl-CoA decarboxylase to the high fatty acid oxidation rates seen in the diabetic heart. *Am. J. Physiol. - Hear. Circ. Physiol.* **278,** 1196–1204 (2000).

37. Finck, B. N. *et al.* The cardiac phenotype induced by PPAR α overexpression mimics that caused by diabetes mellitus. *J. Clin. Invest.* **109,** 121–130 (2002).

38. Chong, C., Clarke, K. & Levelt, E. Metabolic remodelling in diabetic cardiomyopathy. *Cardiovasc. Res.* **113,** 422–430 (2017).

39. Geraldes, P. & King, G. L. Activation of Protein Kinase C Isoforms and Its Impact on Diabetic Complications AGE. *Circ. Res.* 842–853 (2010). doi:10.1161/CIRCRESAHA.110.217117

40. Schilling, J. D. The Mitochondria in Diabetic Heart Failure: From Pathogenesis to Therapeutic Promise. *Antioxid. Redox Signal.* **22,** 1515–1526 (2015).

41. Montaigne, D. *et al.* Myocardial contractile dysfunction is associated with impaired mitochondrial function and dynamics in type 2 diabetic but not in obese patients. *Circulation* **130,** 554–564 (2014).

42. Kota, S. K., Kota, S. K., Jammula, S., Panda, S. & Modi, K. D. Effect of diabetes on alteration of metabolism in cardiac myocytes: therapeutic implications. *Diabetes Technol. Ther.* **13,** 1155–60 (2011).

43. Sivitz, W. I. & Yorek, M. A. Mitochondrial Dysfunction in Diabetes: From Molecular Mechanisms to Functional Significance and Therapeutic Opportunities. *Antioxid. Redox Signal.* **12,** 537–577 (2010).

44. Lilly, L. S. *Pathophysiology of Heart Disease.* (Lippincott Williams & Wilkins, 2011).

45. Pappachan, J. M., Varughese, G. I., Sriraman, R. & Arunagirinathan Joseph Pappachan, G. M. Diabetic cardiomyopathy: Pathophysiology, diagnostic evaluation and management. *World J Diabetes* **4,** 177–189 (2013).

46. Boyer, J. K., Thanigaraj, S., Schechtman, K. B. & Pérez, J. E. Prevalence of ventricular diastolic dysfunction in asymptomatic, normotensive patients with diabetes mellitus. *Am. J. Cardiol.* **93,** 870–875 (2004).

47. Bocchiaro, P. & Zamperini, A. Evaluation of Left Ventricular Diastolic Function by Echocardiography, Establishing Better Standards of Care in Doppler Echocardiography, Computed Tomography and Nuclear Cardiology. *InTech* (2011).

48. Bloch, K. E., Jugoon, S. & Sackner, M. a. Inductance cardiography (thoracocardiography): a novel, noninvasive technique for monitoring left ventricular filling. *J. Crit. Care* **14,** 177–185 (1999).

49. Somaratne, J. B. *et al.* Screening for left ventricular hypertrophy in patients with type 2 diabetes mellitus in the community. *Cardiovasc. Diabetol.* **10,** 1–8 (2011).

50. Eguchi, K. *et al.* Association Between Diabetes Mellitus and Left Ventricular Hypertrophy in a Multiethnic Population. *Am. J. Cardiol.* **101,** 1787–1791 (2008).

51. Atas, H. *et al.* Effects of diabetes mellitus on left atrial volume and functions in normotensive patients without symptomatic cardiovascular disease. *J. Diabetes Complications* **28,** 858–862 (2014).

52. Erdogan, D. *et al.* The effects of good glycaemic control on left ventricular and

coronary endothelial functions in patients with poorly controlled Type 2 diabetes mellitus. *Clin. Endocrinol. (Oxf).* **82,** 388–396 (2015).

53. Nagueh, S. F. *et al.* Recommendations for the Evaluation of Left Ventricular Diastolic Function by Echocardiography: An Update from the American Society of Echocardiography and the European Association of Cardiovascular Imaging. *J. Am. Soc. Echocardiogr.* **29,** 277–314 (2016).

54. Galluzzi, L., Kepp, O., Trojel-Hansen, C. & Kroemer, G. Mitochondrial control of cellular life, stress, and death. *Circ. Res.* **111,** 1198–1207 (2012).

55. Tait, S. W. G. & Green, D. R. Mitochondria and cell signalling. *J. Cell Sci.* **125,** 807–15 (2012).

56. Vandecasteele, G., Szabadkai, G. & Rizzuto, R. Mitochondrial calcium homeostasis: mechanisms and molecules. *IUBMB Life* **52,** 213–219 (2001).

57. Bartz, R. R., Suliman, H. B. & Piantadosi, C. A. Redox mechanisms of cardiomyocyte mitochondrial protection. *Front. Physiol.* **6,** 1–8 (2015).

58. Burté, F., Carelli, V., Chinnery, P. F. & Yu-wai-man, P. Disturbed mitochondrial dynamics and neurodegenerative disorders. *Nat. Publ. Gr.* **11,** 11–24 (2014).

59. Chaturvedi, R. K. & Beal, M. F. Mitochondrial Diseases of the Brain. *Free Radic. Biol. Med.* **63,** 1–29 (2013).

60. Zong, W., Rabinowitz, J. D. & White, E. Mitochondria and Cancer. *Mol. Cell* **61,** 667–676 (2016).

61. Wallace, D. C. Mitochondria and cancer. *Nat. Rev.* **12,** 685–698 (2012).

62. Martin, S. D., Morrison, S., Konstantopoulos, N. & McGee, S. L. Mitochondrial dysfunction has divergent, cell type-dependent effects on insulin action. *Mol. Metab.* **3,** 408–418 (2014).

63. Koves, T. R. *et al.* Mitochondrial Overload and Incomplete Fatty Acid Oxidation Contribute to Skeletal Muscle Insulin Resistance. *Cell Metab.* **7,** 45–56 (2008).

64. Parish, R. & Petersen, K. F. Mitochondrial dysfunction and type 2 diabetes. *Curr. Diab. Rep.* **5,** 177–83 (2005).

65. Tocchetti, C. G. *et al.* GSH or Palmitate Preserves Mitochondrial Energetic/Redox Balance, Preventing Mechanical Dysfunction in Metabolically Challenged Myocytes/Hearts From Type 2 Diabetic Mice. *Diabetes* **61,** 3094–3105 (2012).

66. Falcão-Pires, I. & Leite-Moreira, A. F. Diabetic cardiomyopathy: understanding the molecular and cellular basis to progress in diagnosis and treatment. *Heart Fail. Rev.* **17,** 325–344 (2012).

67. Lou, P.-H. *et al.* Alterations in Fatty Acid Metabolism and Sirtuin Signaling Characterizes Early Type-2 Diabetic Hearts of Fructose-fed Rats. *Physiol. Rep.* 1–58 (2017).

68. W.I., S. & M.A., Y. Mitochondrial dysfunction in diabetes: From molecular mechanisms to functional significance and therapeutic opportunities. *Antioxidants Redox Signal.* **12,** 537–577 (2010).

69. Gnaiger, E. *Mitochondrial Pathways and Respiratory Control: An Introduction to OXPHOS Analysis. Mitochondrial Physiology Network* (2012).

70. Ashrafian, H., Frenneaux, M. P. & Opie, L. H. Metabolic mechanisms in heart failure. *Circulation* **116,** 434–448 (2007).

71. Bremer, J. & Norum, K. R. Metabolism of very long-chain monounsaturated fatty acids (22 : 1) and the adaptation to their presence in the diet. *J. Lipid Res.* **23,** 243–256 (1982).

72. Watmough, N. J. & Frerman, F. E. The electron transfer flavoprotein: Ubiquinone

oxidoreductases. *Biochim. Biophys. Acta - Bioenerg.* **1797,** 1910–1916 (2010).

73. Kresze, G.-B. & Ronft, H. Pyruvate Dehydrogenase Complex from Baker' s Yeast 1. Purification and Some Kinetic and Regulatory Properties. *Eur. J. Biochem.* **119,** 573–579 (1981).

74. Patel, M. S., Nemeria, N. S., Furey, W. & Jordan, F. The pyruvate dehydrogenase complexes: Structure-based function and regulation. *J. Biol. Chem.* **289,** 16615–16623 (2014).

75. Jeoung, N. H. Pyruvate dehydrogenase kinases: Therapeutic targets for diabetes and cancers. *Diabetes Metab. J.* **39,** 188–197 (2015).

76. Aon, M. A., Tocchetti, C. G., Bhatt, N., Paolocci, N. & Cortassa, S. Protective Mechanisms of Mitochondria and Heart Function in Diabetes. *Antioxid. Redox Signal.* **22,** 1563–1586 (2015).

77. Neubauer, S. The Failing Heart — An Engine Out of Fuel. *N. Engl. J. Med.* **356,** 1140–1151 (2007).

78. Barth, E., Stämmler, G., Speiser, B. & Schaper, J. Ultrastructural quantitation of mitochondria and myofilaments in cardiac muscle from 10 different animal species including man. *J. Mol. Cell. Cardiol.* **24,** 669–681 (1992).

79. Palmer, W. Biochemical Properties of Subsarcolemmal and Interfibrillar Mitochondria Isolated from Rat Cardiac Muscle. *Biol. Chem.* **236,** 8731–8739 (1977).

80. Croston, T. L. *et al.* Functional deficiencies of subsarcolemmal mitochondria in the type 2 diabetic human heart. *Am. J. Physiol. Heart Circ. Physiol.* **307,** H54-65 (2014).

81. Bugger, H. *et al.* Type 1 diabetic akita mouse hearts are insulin sensitive but manifest structurally abnormal mitochondria that remain coupled despite increased uncoupling protein 3. *Diabetes* **57,** 2924–2932 (2008).

82. Lashin, O. M., Szweda, P. a., Szweda, L. I. & Romani, A. M. P. Decreased complex II respiration and HNE-modified SDH subunit in diabetic heart. *Free Radic. Biol. Med.* **40,** 886–896 (2006).

83. Dabkowski, E. R. *et al.* Mitochondrial dysfunction in the type 2 diabetic heart is associated with alterations in spatially distinct mitochondrial proteomes. *Am. J. Physiol. Heart Circ. Physiol.* **299,** H529–H540 (2010).

84. Anderson, E. J. *et al.* Substrate-Specific Derangements in Mitochondrial Metabolism and Redox Balance in the Atrium of the Type 2 Diabetic Human Heart. *J. Am. Coll. Cardiol.* **54,** 1891–1898 (2009).

85. Lopaschuk, G. D., Ussher, J. R., Folmes, C. D. L., Jaswal, J. S. & STANLEY, W. C. Myocardial Fatty Acid Metabolism in Health and Disease. *Physiol. Rev.* **90,** 207–258 (2010).

86. Belke, D. D., Larsen, T. S., Gibbs, E. M. & Severson, D. L. Altered metabolism causes cardiac dysfunction in perfused hearts from diabetic (db/db) mice. *Am. J. Physiol. Endocrinol. Metab.* **279,** E1104–E1113 (2000).

87. Koliaki, C. & Roden, M. Alterations of Mitochondrial Function and Insulin Sensitivity in Human Obesity and Diabetes Mellitus. *Annu Rev Nutr* 1–31 (2016). doi:10.1146/annurev-nutr-071715-050656

88. Carley, A. N. & Severson, D. L. Fatty acid metabolism is enhanced in type 2 diabetic hearts. *Biochem. Biophys. Acta* **1734,** 112–126 (2005).

89. Nishikawa, T. *et al.* Normalizing mitochondrial superoxide production blocks three pathways of hyperglycaemic damage. *Nature* **404,** 787–790 (2000).

90. Vazquez, E. J. *et al.* Mitochondrial complex I defect and increased fatty acid oxidation enhance protein lysine acetylation in the diabetic heart. *Cardiovasc. Res.* **107,** 453–465

(2015).

91. Yu, T., Robotham, J. & Yoon, Y. Increased production of reactive oxygen species in hyperglycemic conditions requires dynamic change of mitochondrial morphology. *Proc. Natl. Acad. Sci. U. S. A.* **103,** 2653–2658 (2006).

92. Yan, W. *et al.* Impaired mitochondrial biogenesis due to dysfunctional adiponectin-AMPK-PGC-1 a signaling contributing to increased vulnerability in diabetic heart. *Basic Res. Cardiol.* **329,** 1–15 (2013).

93. Hütter, E., Unterluggauer, H., Garedew, A., Jansen-Dürr, P. & Gnaiger, E. High-resolution respirometry-a modern tool in aging research. *Exp. Gerontol.* **41,** 103–109 (2006).

94. Gnaiger, E. Polarographic Oxygen Sensors, the Oxygraph, and High-Resolution Respirometry to Assess Mitochondrial Function. *Drug-Induced Mitochondrial Dysfunct.* 325–352 (2008). doi:10.1002/9780470372531.ch12

95. Gnaiger, E. The Oxygraph for High Resolution Respirometry (HRR). *Mitochondrial Physiol. Netw.* **6,** 1–18 (2011).

96. Islam, M. S. & Wilson, R. D. *Experimentally induced rodent models of type 2 diabetes. Methods in molecular biology (Clifton, N.J.)* **933,** (2012).

97. Jones, S. P. *et al.* Reperfusion injury is not affected by blockade of P-selectin in the diabetic mouse heart are lost in the setting of obesity and diabetes. *Physiol, Am J Circ, Hear.* 763–769 (1999).

98. Rerup, C. C. Drugs producing diabetes through damage of the insulin secreting cells. *Pharmacol. Rev.* **22,** 485–518 (1970).

99. Szkudelski, T. The mechanism of alloxan and streptozotocin action in B cells of the rat pancreas. *Physiol. Res.* **50,** 537–546 (2001).

100. Reed, M. J. *et al.* A new rat model of type 2 diabetes: The fat-fed, streptozotocin-treated rat. *Metabolism.* **49,** 1390–1394 (2000).

101. Noda, K. *et al.* An animal model of spontaneous metabolic syndrome: Nile grass rat. *FASEB J.* **24,** 2443–2453 (2010).

102. Rabiu, S. & Rose, R. K. A quantitative study of diet in three species of rodents in natural and irrigated savanna fields. *Acta Theriol. (Warsz).* **42,** 55–70 (1997).

103. Schrader, J. A., Walaszczyk, E. J. & Smale, L. Changing patterns of daily rhythmicity across reproductive states in diurnal female Nile grass rats (Arvicanthis niloticus). *Physiol. Behav.* **98,** 547–556 (2009).

104. Castillo-Ruiz, A., Nixon, J. P., Smale, L. & Nunez, A. A. Neural activation in arousal and reward areas of the brain in day-active and night-active grass rats. *Neuroscience* **165,** 337–349 (2010).

105. Bobu, C. *et al.* Photoreceptor Organization and Rhythmic Phagocytosis in the Nile Rat Arvicanthis Ansorgei: A Novel Diurnal Rodent Model for the Study of Cone Pathophysiology. *Invest Ophthalmol Vis Sci* **47,** 3109–3118 (2010).

106. Chaabo, F., Pronczuk, A., Maslova, E. & Hayes, K. Nutritional correlates and dynamics of diabetes in the Nile rat (Arvicanthis niloticus): a novel model for diet-induced type 2 diabetes and the metabolic syndrome. *Nutr. Metab. (Lond).* **7,** 29 (2010).

107. Yang K, Gotzmann J, Kuny S, Huang H, Sauve Y, C. C. *Five stages of progressive beta-cell dysfunction in the laboratory Nile rat model of type 2*. (2016).

108. Weir, G. C. & Bonner-Weir, S. Five of stages of evolving beta-cell dysfunction during progression to diabetes. *Diabetes* **53,** (2004).

109. Goldstein, R. E. *et al.* Effects of chronic elevation in plasma cortisol on hepatic carbohydrate metabolism. *Am. J. Physiol. Endocrinol. Metab.* (1993).

110. Han, W. H. *et al.* Modifications in Retinal Mitochondrial Respiration Precede Type 2 Diabetes and Protracted Microvascular Retinopathy e. *Investig. Ophthalmol. Vis. Sci.* 1–15 (2017). doi:10.1167/iovs.17-21929

111. Dolinsky, V. W. *et al.* Both aerobic exercise and resveratrol supplementation attenuate doxorubicin-induced cardiac injury in mice. *Am. J. Physiol. Endocrinol. Metab.* **305,** 243–253 (2013).

112. Dolinsky, V. W. *et al.* Calorie Restriction Prevents Hypertension and Cardiac Hypertrophy in the Spontaneously Hypertensive Rat. *Hypertension* **56,** 412–421 (2010).

113. Lemieux, H., Semsroth, S., Antretter, H., Höfer, D. & Gnaiger, E. Mitochondrial respiratory control and early defects of oxidative phosphorylation in the failing human heart. *Int. J. Biochem. Cell Biol.* **43,** 1729–38 (2011).

114. Lemieux, H., Blier, P. U. & Gnaiger, E. Remodeling pathway control of mitochondrial respiratory capacity by temperature in mouse heart : electron flow through the Q-junction in permeabilized fibers. *Sci. Rep.* 1–13 (2017). doi:10.1038/s41598-017-02789-8

115. Saks, V. A. Mitochondrial respiratory parameters in cardiac tissue : a novel method of assessment by using saponin-skinned fibers Vladimir I . Veksler , Andrey V . Kuznetsov , Victor G . Sharov , Valery I . Kapelko. *Biochem. Biophys. Acta* **892,** 191–196 (1987).

116. Gnaiger, E., Kuznetsov, A.V., Schneeberger, S., Seiler, R., Brandacher, G., Steurer, W., Margreiter, R. in *Life in the Cold* 431–442 (Springer Berlin Heidelberg, 2000).

117. Pesta, D. & Gnaiger, E. *Mitochondrial Bioenergetics*. **810,** (2012).

118. Gnaiger, E., Lassnig, B., Kuznetsov, A., Reiger, G., M. R. Mitochondrial Oxygen Affinity, Respiratory Flux Control, and Excess Capacity of Cytochrome c oxidase. *J.*

Exp. Biol. **1139,** 1129–1139 (1998).

119. Gnaiger, E., Steinlechner-maran, R., Mendez, G., Eberl, T. & Margreiter, R. Control of Mitochondrial and Cellular Respiration by Oxygen. *J. Bioenerg. Biomembr.* **27,** (1995).

120. Harrison, D. K., Fasching, M., Fontana-ayoub, M. & Gnaiger, E. Cytochrome redox states and respiratory control in mouse and beef heart mitochondria at steady-state levels of hypoxia. *J. Appl. Physiol.* **119,** 1210–1218 (2015).

121. Salabei, J. K., Gibb, A. A. & Hill, B. G. Comprehensive measurement of respiratory activity in permeabilized cells using extracellular flux analysis. *Nat. Protoc.* **9,** 421–438 (2014).

122. Papamandjaris, A. A., Macdougall, D. E. & Jones, P. J. H. Medium Chain Fatty Acid Metabolism and Energy Expenditure : Obesity Treatment Implications. *Life Sci.* **62,** 1203–1215 (1998).

123. Ojuka, E. *et al.* Measurement of B-oxidation capacity of biological samples by respirometry : a review of principles and substrates. *Am. J. Physiol. Endocrinol. Metab.* **310,** 715–723 (2016).

124. Larsen, S. *et al.* Biomarkers of mitochondrial content in skeletal muscle of healthy young human subjects. *J. Physiol.* **14,** 3349–3360 (2012).

125. Kuznetsov, A. V, Lassnig, B. & Gnaiger, E. Citrate Synthase: Mitochondrial Marker Enzyme. *Mitochondrial Physiol. Netw.* **4,** 1–10 (2010).

126. Faloona, G. R. & Srere, P. A. Escherichia coli Citrate Synthase. Purification and the Effect of Potassium on Some Properties. *Biochemistry* **8,** 4497–4503 (1969).

127. Vazquez, E. J., Fujioka, H. & Hoppel, C. L. Decrease in Mitochondrial Function in Rat Cardiac Permeabilized Fibers Correlates With the Aging Phenotype. *J. Gerontol.* 1157–1164 (2010). doi:10.1093/gerona/glq141

128. Pierozan, P., Jerneren, F., Ransome, Y. & Oskar Karlsson. The Choice of Euthanasia Method Affects Metabolic Serum Biomarkers. *Basic Clin. Pharmacol. Toxicol.* **121,** 113–118 (2017).

129. Sorlini, M. & Benini, F. Hypoglycemia , an Atypical Early Sign of Hepatocellular Carcinoma. *J. Gastrointest. Cancer* **41,** 209–211 (2010).

130. Iglesias, P. & Dıez, J. J. Management of Endocrine Disease: A Clinical Update on Tumor-Induced Hypoglycemia. *Eur. J. Endocrinol.* **170,** 147–157 (2014).

131. Fink, R. I., Kolterman, O. G. & Griffin, J. Mechanisms of Insulin Resistance in Aging. *J. Clin. Invest.* **71,** 1523–1535 (1983).

132. DeFronzo, R. Glucose Intolerance and Aging. *Diabetes Care* **4,** 493–501 (1981).

133. Lyall, D. M. *et al.* Association of Body Mass Index With Cardiometabolic Disease in the UK Biobank A Mendelian Randomization Study. *JAMA Cardiol.* (2017). doi:10.1001/jamacardio.2016.5804

134. Mostarda, C. T. *et al.* Low intensity resistance training improves systolic function and cardiovascular autonomic control in diabetic rats. *J. Diabetes Complications* **28,** 273–278 (2014).

135. Vinik, A. I., Erbas, T. & Casellini, C. M. Diabetic cardiac autonomic neuropathy , inflammation and cardiovascular disease. *J. Diabetes Investig.* **4,** (2013).

136. Vinik, A. I., Maser, R. E. & Ziegler, D. Autonomic imbalance : prophet of doom or scope for hope? *Diabet. Med.* **28,** 643–651 (2011).

137. Dyrby, N., Biering-sørensen, T., Jensen, S. & Mogelvang, R. Diastolic dysfunction revisited : A new , feasible , and unambiguous echocardiographic classification predicts major cardiovascular events. *Am. Heart J.* **188,** 136–146 (2017).

138. Liu, J. & Rigel, D. F. in *Cardiovascular Genomics, Methods in Molecular Biology* 139–155

(2009). doi:10.1007/978-1-60761-247-6

139. Nagueh, S. F. E / e ' Ratio : An Index of LV Filling Pressures Revisited. 56 (2013).

140. Ho, C. Y. & Solomon, S. D. A Clinician's Guide to Tissue Doppler Imaging. *Circulation* **113,** 396–399 (2006).

141. Boushel, R., Gnaiger, E., Schjerling, P. & Skovbro, M. Patients with type 2 diabetes have normal mitochondrial function in skeletal muscle. *Diabetologia* **50,** 790–796 (2007).

142. De Pauw, A., Tejerina, S., Raes, M., Keijer, J. & Arnould, T. Mitochondrial (Dys)function in Adipocyte (De)differentiation and Systemic Metabolic Alterations. *Am. J. Pathol.* **175,** 927–939 (2009).

143. Cheng, Z. *et al.* Foxo1 integrates insulin signaling with mitochondrial function in the liver. *Nat. Med.* **15,** 1307–1312 (2009).

144. Mitra, R. *et al.* The transcriptional coactivators , PGC-1 α and β , cooperate to maintain cardiac mitochondrial function during the early stages of insulin resistance. *J. Mol. Cell. Cardiol.* **52,** 701–710 (2012).

145. Boudina, S. & Abel, E. D. Mitochondrial Uncoupling : A Key Contributor to Reduced Cardiac Efficiency in Diabetes. *Physiology* **21,** 250–258 (2006).

146. Boudina, S. *et al.* Reduced Mitochondrial Oxidative Capacity and Increased Mitochondrial Uncoupling Impair Myocardial Energetics in Obesity. *Circulation* **112,** 2686–2695 (2005).

147. Duncan, J. G., Fong, J. L., Medeiros, D. M., Finck, B. N. & Kelly, D. P. Insulin-Resistant Heart Exhibits a Mitochondrial Biogenic Response Driven by the Peroxisome Proliferator-Activated. *Circulation* **115,** 909–917 (2007).

148. Sivasinprasasn, S. *et al.* Obese-insulin resistance accelerates and aggravates

cardiometabolic disorders and cardiac mitochondrial dysfunction in estrogen-deprived female rats. *Age (Omaha).* **37,** (2015).

149. Morrow, R. M. *et al.* Mitochondrial energy deficiency leads to hyperproliferation of skeletal muscle mitochondria and enhanced insulin sensitivity. *Proc. Natl. Acad. Sci. U. S. A.* (2017). doi:10.1073/pnas.1700997114

150. Noble, E. G. *et al.* Influence of training on skeletal muscle enzymatic adaptations in normal and diabetic rats. *Am. Physiol. Soc.* (1985).

151. Yoon, Y. & Galloway, C. A. Mitochondrial Dynamics in Diabetes. *Antioxid. Redox Signal.* **14,** (2011).

152. Parone, P. A., James, D. I., Cruz, S. Da & Mattenberger, Y. Inhibiting the Mitochondrial Fission Machinery Does Not Prevent Bax/Bak-Dependent Apoptosis. *Mol. Cell. Biol.* **26,** 7397–7408 (2006).

153. Jastroch, M., Divakaruni, A. S., Mookerjee, S., Treberg, J. R. & Brand, M. D. Mitochondrial proton and electron leaks. *Essays Biochem.* **47,** 53–67 (2010).

154. Nicholls, D. G. The Non-Ohmic Proton Leak — 25 Years On. *Biosci. Rep.* **17,** 251–257 (1997).

155. Brookes, P. S. Mitochondrial H(+) leak and ROS generation: an odd couple. *Free Radic. Biol. Med.* **38,** 12–23 (2005).

156. Boudina, S. *et al.* Mitochondrial Energetics in the Heart in Obesity-Related Diabetes: Direct Evidence for Increased Uncoupled Respiration and Activation of Uncoupling Proteins. *Diabetes* **56,** 2457–2466 (2007).

157. Boss, O. *et al.* Uncoupling protein-3 : a new member of the mitochondrial carrier family with tissue-specific expression. *FEBS Lett.* **408,** 39–42 (1997).

158. Moore, G. B. T., Himms-hagen, J., Harper, M. & Clapham, J. C. Overexpression of

UCP-3 in Skeletal Muscle of Mice Results in Increased Expression of Mitochondrial Thioesterase mRNA. *Biochem. Biophys. Res. Commun.* **790,** 785–790 (2001).

159. Olesch, M., Giessen, S., Pauschinger, M. & Schultheiss, H. Transcription of the adenine nucleotide translocase isoforms in various types of tissues in the rat. *Biochem. Biophys. Acta* **1417,** 16–24 (1999).

160. Hsueh, W. *et al.* Recipes for creating animal models of diabetic cardiovascular disease. *Circ. Res.* **100,** 1415–1427 (2007).

161. Franko, A. *et al.* Liver adapts mitochondrial function to insulin resistant and diabetic states in mice. *J. Hepatol.* **60,** 816–823 (2014).

162. Green, K., Brand, M. D. & Murphy, M. P. Prevention of Mitochondrial Oxidative Damage as a Therapeutic Strategy in Diabetes. *Diabetes* **53,** (2004).

163. Serviddio, G. *et al.* Bioenergetics in aging : mitochondrial proton leak in aging rat liver , kidney and heart. *Redox Rep.* **12,** 91–95 (2007).

164. Payne, B. A. I. & Chinnery, P. F. Mitochondrial dysfunction in aging : Much progress but many unresolved questions. *BBA - Bioenerg.* **1847,** 1347–1353 (2015).

165. Mecocci, P. *et al.* Age-Dependent Increases In Oxidative Damage To DNA, Lipids, and Proteins in Human Skeletal Muscle. *Free Radic. Biol. Med.* **26,** 303–308 (1999).

166. Greaves, L. C. *et al.* Quantification of mitochondrial DNA mutation load. *Aging Cell* **8,** 566–572 (2009).

167. Mendoza-Núñez, V. M., Ruiz-Ramos, M., Sánchez-Rodríguez, M. a, Retana-Ugalde, R. & Muñoz-Sánchez, J. L. Aging-related oxidative stress in healthy humans. *Tohoku J. Exp. Med.* **213,** 261–268 (2007).

168. Malhotra, A. *et al.* Inhibition of p66ShcA redox activity in cardiac muscle cells attenuates hyperglycemia-induced oxidative stress and apoptosis. *Am. J. Physiol. - Hear.*

Circ. Physiol. **7103,** 380–388 (2009).

169. Hoehn, K. L. *et al.* Insulin resistance is a cellular antioxidant defense mechanism. *PNAS* **106,** 17787–17792 (2010).

170. Vanhoose, L. *et al.* Time-Dependent Alterations in Rat Macrovessels with Type 1 Diabetes Time-Dependent Alterations in Rat Macrovessels with Type 1 Diabetes. *Exp. Diabates Res.* (2012). doi:10.1155/2012/278620

171. Bhashyam, S. *et al.* Aging is associated with myocardial insulin resistance and mitochondrial dysfunction. *Am. J. Physiol. - Hear. Circ. Physiol.* **19104,** 3063–3071 (2007).

172. Rossignol, R. *et al.* Mitochondrial threshold effects. *Biochem. J.* **762,** 751–762 (2003).

173. Constantin-Teodosiu, D. Regulation of Muscle Pyruvate Dehydrogenase Complex in Insulin Resistance : Effects of Exercise and Dichloroacetate. *Diabetes Metab. J.* **37,** 301–314 (2013).

174. Ahuja, P. *et al.* Divergent Mitochondrial Biogenesis Responses in Human Cardiomyopathy. *Circulation* **127,** 1957–1967 (2013).

175. Xu, X. J., Babo, E., Qin, F., Croteau, D. & Colucci, W. S. Short-term caloric restriction in db / db mice improves myocardial function and increases high molecular weight (HMW) adiponectin. *IJCME* **13,** 28–34 (2016).

176. Lanza, I. R. *et al.* Chronic Caloric Restriction Preserves Mitochondrial Function in Senescence without Increasing Mitochondrial Biogenesis. *Cell Metab.* **16,** 777–788 (2012).

177. Takasawa, M. & Hayakawa, M. Age-Associated Damage In Mitochondrial Function in Rat Hearts. *Exp. Gerontol.* **28,** 269–280 (1993).

178. Short, K. R. *et al.* Decline in skeletal muscle mitochondrial function with aging in

humans. *Proc. Natl. Acad. Sci. U. S. A.* **102,** 5618–5623 (2005).

179. Lee, H.-C. & Wei, Y.-H. in *Advances in Mitochondrial Medicine* 311–328 (Springer Berlin Heidelberg, 2011).

180. Nakamura, S. *et al.* Palmitate Induces Insulin Resistance in H4IIEC3 Hepatocytes through Reactive Oxygen Species Produced. *J. Biol. Chem.* **284,** 14809–14818 (2009).

181. Gomes, A. P. *et al.* Declining NAD + Induces a Pseudohypoxic State Disrupting Nuclear-Mitochondrial Communication during Aging. *Cell* **155,** 1624–1638 (2013).

182. Shadel, G. S. Aging : It's SIRTainly Possible to Restore Mitochondrial Dysfunction. *Curr. Biol.* **24,** R206–R208 (2013).

183. Kitada, M. & Koya, D. SIRT1 in Type 2 Diabetes : Mechanisms and Therapeutic Potential. *Diabetes Metab.* **37,** 315–325 (2013).

184. Bourens, M. & Fontanesi, F. Redox and Reactive Oxygen Species Regulation. *Antioxidants Redox Signal.* **19,** 1940–1952 (2013).

185. Srinivasan, S. & Avadhani, N. G. Cytochrome c oxidase dysfunction in oxidative stress. *Free Radic. Biol. Med.* **53,** 1252–1263 (2012).

186. Friday, D. P., Alleyne, T. A., Ignacio, D. N. & Arrindell, D. The Impact of Diabetes Mellitus on Oxygen Utilization by Complex IV : Preliminary Insights. *J. Endocrinol. Metab.* **7,** 18–24 (2017).

187. Quagliariello, E. Age-dependent decrease in the cytochrome c oxidase activity and changes in phospholipids in rat-heart mitochondria. *Arch. Gerontol. Geriatr.* **16,** 263–272 (1993).

188. Deepa, S. S. *et al.* Improved insulin sensitivity associated with reduced mitochondrial complex IV assembly and activity. *FASEB J.* **27,** 1371–1380 (2017).

189. Turner, N. *et al.* Excess Lipid Availability Increases Mitochondrial Fatty Acid

Oxidative Capacity in Muscle. *Diabetes* **56,** 2085–2092 (2007).

190. Gupte, A. A. *et al.* High-Fat Feeding-Induced Hyperinsulinemia Increases Cardaic Glucose Uptake and Mitochondrial Function Despite Peripheral Insulin Resistance. *Endocrinology* **154,** 2650–2662 (2013).

191. Wilson, C. R., Tran, M. K., Salazar, K. L., Young, M. E. & Taegtmeyer, H. Western diet , but not high fat diet , causes derangements of fatty acid metabolism and contractile dysfunction in the heart of Wistar rats. *Biochem. Soc.* **467,** 457–467 (2007).

192. Mansor, L. S. *et al.* Cardiac metabolism in a new rat model of type 2 diabetes using high-fat diet with low dose streptozotocin. *Cardiovasc. Diabetol.* **136,** 1–10 (2013).

193. Chen, J. C. & Sanadi, D. R. A. O. Regulation of Mitochondrial Respiration in Senescence. *J. Cell. Physiol.* 141–148 (1970).

194. Fannin, S. W., Lesnefsky, E. J., Slabe, T. J., Hassan, M. O. & Hoppel, C. L. Aging Selectively Decreases Oxidative Capacity in Rat Heart Interfibrillar Mitochondria. *Arch. Biochem. Biophys.* **372,** 399–407 (1999).

195. Muscari, C., Caldarera, C. M. & Guarnieri, C. Age-dependent production of mitochondrial hydrogen peroxide , lipid peroxides and fluorescent pigments in the rat heart. *Basic Res. Cardiol.* **178,** 172–178 (1990).

196. Fisher-Wellman, K. H. & Neufer, P. D. Linking mitochondrial bioenergetics to insulin resistance via redox biology. *Trends Endocrinol. Metab.* **23,** 142–153 (2012).

197. St-Pierre, J., Buckingham, J. A., Roebuck, S. J. & Brand, M. D. Topology of Superoxide Production from Different Sites in the Mitochondrial Electron Transport Chain. *J. Biol. Chem.* **277,** 44784–44790 (2002).